PIC1, an Ancient Permease in *Arabidopsis* Chloroplasts, Mediates Iron Transport [W]

Daniela Duy,[a] Gerhard Wanner,[a] Anderson R. Meda,[b] Nicolaus von Wirén,[b] Jürgen Soll,[a] and Katrin Philippar[a,1]

[a] Department für Biologie 1, Botanik, Ludwig-Maximilians-Universität München, D-80638 Munich, Germany
[b] Molecular Plant Nutrition, Institute for Plant Nutrition, University of Hohenheim, D-70599 Stuttgart, Germany

In chloroplasts, the transition metals iron and copper play an essential role in photosynthetic electron transport and act as cofactors for superoxide dismutases. Iron is essential for chlorophyll biosynthesis, and ferritin clusters in plastids store iron during germination, development, and iron stress. Thus, plastidic homeostasis of transition metals, in particular of iron, is crucial for chloroplast as well as plant development. However, very little is known about iron uptake by chloroplasts. *Arabidopsis thaliana* PERMEASE IN CHLOROPLASTS1 (PIC1), identified in a screen for metal transporters in plastids, contains four predicted α-helices, is targeted to the inner envelope, and displays homology with cyanobacterial permease-like proteins. Knockout mutants of *PIC1* grew only heterotrophically and were characterized by a chlorotic and dwarfish phenotype reminiscent of iron-deficient plants. Ultrastructural analysis of plastids revealed severely impaired chloroplast development and a striking increase in ferritin clusters. Besides upregulation of ferritin, *pic1* mutants showed differential regulation of genes and proteins related to iron stress or transport, photosynthesis, and Fe-S cluster biogenesis. Furthermore, PIC1 and its cyanobacterial homolog mediated iron accumulation in an iron uptake–defective yeast mutant. These observations suggest that PIC1 functions in iron transport across the inner envelope of chloroplasts and hence in cellular metal homeostasis.

INTRODUCTION

Some transition metals, and in particular iron, are essential micronutrients in plants. Thus, to control metal homeostasis, plants have developed specified strategies for metal ion acquisition, distribution to organs and tissues, and subcellular compartmentalization (for overview, see Hall and Williams, 2003; Curie and Briat, 2003; Colangelo and Guerinot, 2006). Dicotyledonous plants such as *Arabidopsis thaliana* take up ferrous iron [Fe(II)] after reduction of Fe(III) chelates from the soil. This first step is accomplished by the action of the plasmalemma root ferric chelate reductase FERRIC REDUCTASE/OXIDASE2 (Robinson et al., 1999) and the major root metal transporter IRON-REGULATED TRANSPORTER1 (IRT1) (Eide et al., 1996; Henriques et al., 2002; Varotto et al., 2002; Vert et al., 2002), which mediates Fe^{2+} uptake into root epidermis cells. Distribution of iron in the plant is achieved by long-distance transport of Fe chelates in the vasculature. A strong chelator of iron is the aminocarboxylate nicotianamine, and members of the YELLOW STRIPE1-LIKE (YSL) transporter family in *Arabidopsis* are likely candidates that contribute to iron distribution by loading and unloading Fe-nicotianamine from the vascular tissue (Le Jean et al., 2005; Waters et al., 2006). Within the plant cell, iron has to be compartmentalized into different organelles, such as chloroplasts, mitochondria, and vacuoles. However, to date, only two members of the NRAMP

(for natural resistance-associated macrophage protein) family of metal transporters, NRAMP3 and NRAMP4, have been shown to play a role in Fe mobilization from the vacuole during seedling development (Thomine et al., 2003; Lanquar et al., 2005). The iron transport pathway across the envelopes of chloroplasts and mitochondria remains unknown, although chloroplasts in particular represent a major sink for metal ions (see below).

Chloroplasts are organelles enclosed by an outer and an inner envelope membrane and have evolved from the endosymbiosis of free-living cyanobacteria with an ancient eukaryotic cell (for review, see Vothknecht and Soll, 2005). Because chloroplasts are the site of photosynthesis, they provide the basis for life on earth in its present form. However, chloroplasts represent only one type of the plastid organelle family in higher plants (for overview, see Möller, 2005). Proplastids in meristematic tissue and etioplasts in dark-grown plantlets develop into the mature, autotrophic chloroplast of the green leaf. By contrast, storage plastids are heterotrophic organelles that convert photosynthates derived from source tissues into storage compounds. Thus, in addition to photosynthesis, plastids harbor many more vital biosynthetic functions, such as nitrogen and sulfur assimilation or the biosynthesis of fatty acids and aromatic amino acids. In consequence, these functions require an active solute exchange across the outer and inner envelope membranes surrounding the chloroplast stroma. Metal transport proteins in both membrane systems thus provide a bottleneck to the control of metal homeostasis in the chloroplast as well as in the plant cell.

Because of their potential for valency changes, the transition metals Fe, Cu, and Mn play a vital role in photosynthetic electron transport in chloroplasts (Raven et al., 1999). Whereas the photosynthetic apparatus represents one of the most iron-enriched systems in the plant cell (photosystem II, photosystem I, cytochrome b_6-f complex, and ferredoxin), copper ions catalyze

electron transfer via plastocyanin and a cluster of Mn atoms is required as the catalytic center in the oxygen-evolving complex. Furthermore, stroma-localized Fe and Cu/Zn superoxide dismutases scavenge reactive oxygen species in the water–water cycle (Kliebenstein et al., 1998; Asada, 1999). In addition, Zn is known to function as a cofactor (RNA polymerase, zinc finger domains) in plastid transcription. During germination, development, and iron stress, ferritin clusters in plastids serve as iron stores (Briat et al., 1999; Connolly and Guerinot, 2002). Furthermore, Fe-S cluster biogenesis in chloroplasts requires the import of iron. Fe-S cluster proteins are essential components of the photosynthetic electron transport chain and are involved in protein import, chlorophyll biosynthesis, and breakdown as well as in nitrogen and sulfur assimilation (for overview of Fe-S biogenesis, see Balk and Lobreaux, 2005; Ye et al., 2006).

Despite these essential functions for metal ions in chloroplasts, very little is known about metal transport proteins in plastid envelopes. To date, the only chloroplast proteins demonstrated to be involved in metal ion transport are the copper-transporting P-type, heavy-metal ATPases PAA1, PAA2, and HMA1 as well as the magnesium transport protein MRS2-11 (Shikanai et al., 2003; Abdel-Ghany et al., 2005; Drummond et al., 2006; Seigneurin-Berny et al., 2006). Whereas PAA1, HMA1, and MRS2-11 have been reported to be localized in the inner chloroplast envelope, PAA2 transports Cu across the thylakoid membrane. Direct measurements of iron transport on isolated pea (*Pisum sativum*) chloroplasts have shown that iron is transported in the ferrous form across the inner envelope (Shingles et al., 2001, 2002). Fe^{2+} uptake into chloroplasts is most likely energized by a proton gradient and can be inhibited by Zn^{2+}, Cu^{2+}, or Mn^{2+}. The putative metal uptake protein might thus mediate Fe^{2+}/H^+-uniport and be able to transport Zn^{2+}, Cu^{2+}, and Mn^{2+} as well.

In this study, we characterized PERMEASE IN CHLOROPLASTS1 (PIC1), a transmembrane protein in the inner envelope of *Arabidopsis* chloroplasts. PIC1 is of cyanobacterial origin and most likely functions in iron permease in the chloroplast envelope. The detailed characterization of *pic1* knockout mutants reveals a phenotype reminiscent of iron-deficient chloroplasts. This includes chlorosis, an altered organization of leaf mesophyll cells, and severe defects in chloroplast and thylakoid development. These findings are supported by differential gene expression in *pic1* mutants (e.g., downregulation of genes involved in photosynthesis and Fe-S cluster biogenesis). By contrast, the accumulation of ferritin clusters in *pic1* mutant plastids as well as the upregulation of stress-related genes indicates an iron-overload reaction in the cytosol and impaired metal homeostasis at the cellular level. Because PIC1 and its cyanobacterial homolog sll1656 were able to complement the growth of an iron uptake–defective yeast mutant and to confer iron uptake, we conclude that the protein is involved in iron transport and homeostasis in chloroplasts.

RESULTS

A Putative Permease of Cyanobacterial Origin in Chloroplast Envelopes

In our search for potential metal ion transporters in plastid envelopes, we screened the *Arabidopsis* chloroplast proteome for polypeptides that are hydrophobic, have a basic isoelectric point, contain potential transmembrane domains, and show significant homology with cyanobacterial proteins. The protein At2g15290 was identified in a mixed envelope preparation of *Arabidopsis* chloroplasts (Froehlich et al., 2003) and according to in silico analyses was classified into the virtual hydrophobic proteome from plastid envelope membranes (Rolland et al., 2003). Furthermore, a screening of publicly available databases revealed outstanding similarities to cyanobacterial proteins (Figure 1A). To date, the function of all proteins homologous with At2g15290 is annotated as unknown; however, some cyanobacterial proteins were grouped into prokaryotic clusters of orthologous groups of proteins (COGs) (Tatusov et al., 2003). Among these COGs were high-affinity Fe^{2+}/Pb^{2+} permeases, permease components of major facilitator proteins and ABC-type (for ATP binding cassette) transport systems or amino acid transporters, indicating that At2g15290 might function as a permease in solute transport across the plastid envelope membranes. Thus, in this report, we refer to At2g15290 as PIC1 (for PERMEASE IN CHLOROPLASTS1).

According to the ARAMEMNON database (Schwacke et al., 2003), PIC1 represents a chloroplast-localized membrane protein with four α-helical transmembrane domains. The predicted topology is depicted in Figures 1B and 1C. In *Arabidopsis*, the nucleus-encoded PIC1 represents a single-copy gene with no further homologs identified. A BLAST search against plant sequences in GenBank and PHYSCObase identified one homolog in *Lotus corniculatus* var *japonicus*, two genes in each of the monocots *Oryza sativa* and *Zea mays*, and one homologous protein in the moss *Physcomitrella patens* (Figure 1A). A chloroplast-targeting signal peptide as well as four α-helical transmembrane domains are predicted for all plant proteins, and the mature polypeptide chains of this unique family are highly similar (60 to 74% amino acid identity) (Figure 1C; see Supplemental Figure 1 online).

The amino acid sequence of the mature PIC1, to our surprise, showed significant homology only with proteins of cyanobacterial origin. The protein with the highest similarity (24% amino acid identity) is encoded by the gene *sll1656* in *Synechocystis* sp PCC 6803 (Figure 1C). The sole eukaryotic relatives except in vascular plants were found in the genomes of the green alga *Chlamydomonas reinhardtii* and the red alga *Cyanidioschyzon merolae* (Figure 1A). Thus, PIC1 seems to originate directly from the endosymbiosis of a cyanobacterium with a eukaryotic cell, which led to the formation of chloroplasts (Vothknecht and Soll, 2005). Except in the ancient cyanobacterium *Gloeobacter violaceus*, at least one homolog was present in all sequenced cyanobacterial genomes. Interestingly, *Gloeobacter* is the only genus lacking a thylakoid membrane system (Nakamura et al., 2003).

PIC1 Is Localized in the Inner Envelope of *Arabidopsis* Chloroplasts

To verify the predicted chloroplast localization of PIC1, we performed in vitro import experiments into isolated *Arabidopsis* chloroplasts. The precursor protein PIC1 was imported into isolated intact chloroplasts of 8-d-old seedlings and processed to a mature protein of ~22 kD (Figure 2A). The protein was resistant to protease treatment, confirming import into chloroplasts. In
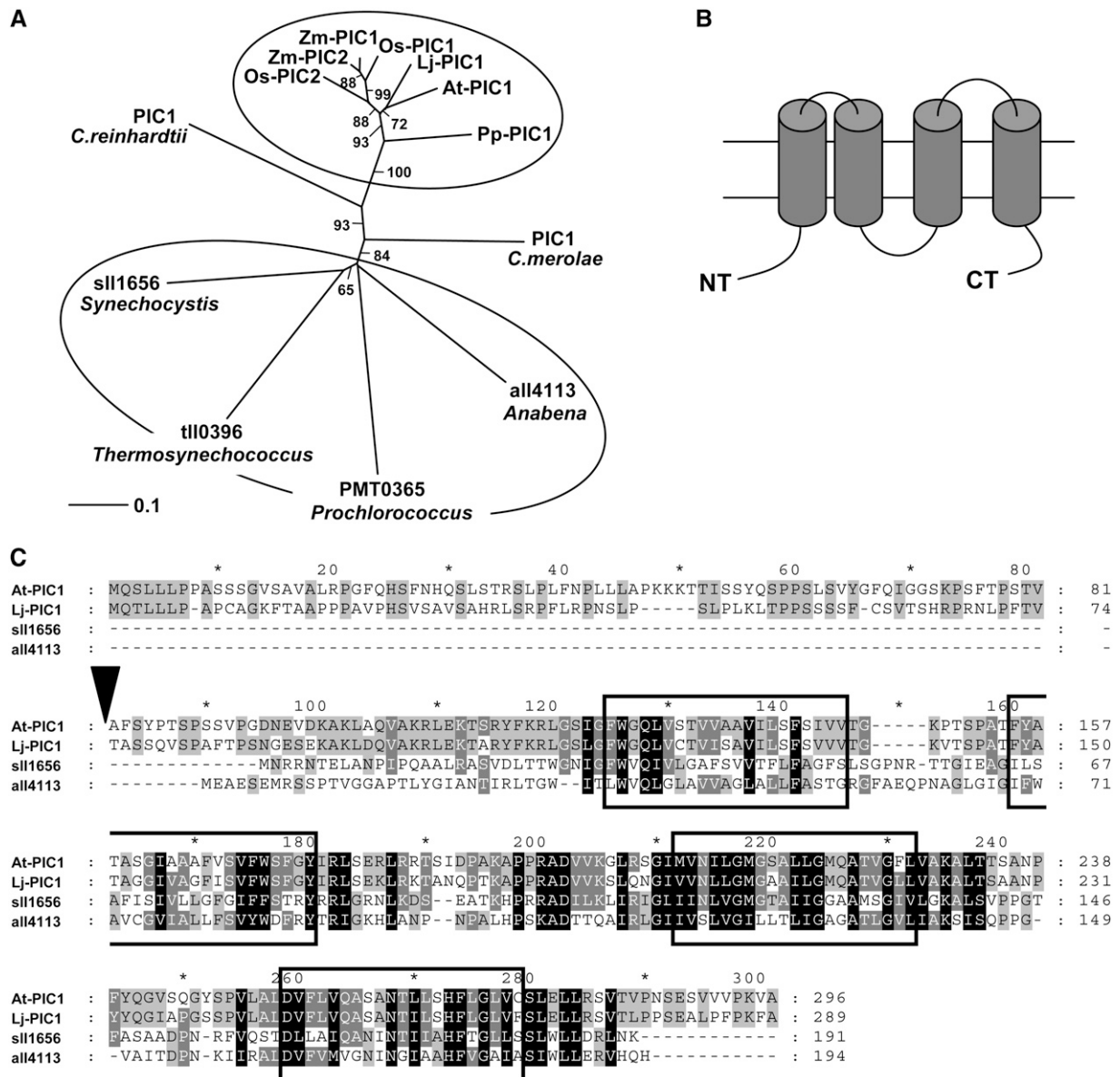
Figure 1. PIC1 Is a Permease of Cyanobacterial Origin with Four α-Helical Transmembrane Domains.

(A) Phylogenetic tree of the PIC family in eukaryotes and cyanobacteria. In plants, At-PIC1 groups into a family of homologous proteins from monocots such as rice (Os-PIC1 and Os-PIC2) and maize (Zm-PIC1 and Zm-PIC2). The closest relative to At-PIC1 is found in the dicotyledonous plant *Lotus japonicus* (Lj-PIC1), whereas the homolog from the moss *Physcomitrella patens* (Pp-PIC1) is more distantly related. In the genomes of the green alga *Chlamydomonas reinhardtii* as well as the red alga *Cyanidioschyzon merolae*, we could identify homologs to At-PIC1. Cyanobacterial relatives to At-PIC1 from *Synechocystis* sp PCC 6803 (sll1656), *Anabena* sp PCC 7120 (all4113), *Thermosynechococcus elongatus* BP-1 (tll0396), and *Prochlorococcus marinus* strain MIT 9313 (PMT0365) are depicted. All proteins were identified by BLAST screening of At-PIC1 against the respective databases (see Methods). The distance tree is based on 148 amino acids of the predicted mature proteins (see Methods and Supplemental Figure 1 online). Bootstrap values for the respective branches are indicated.
(B) Predicted topology for PIC1. According to the AM consensus prediction (ARAMEMNON database; Schwacke et al., 2003), four α-helical transmembrane domains are proposed for At-PIC1 as well as for the homologs Os-PIC1, Os-PIC2, sll1656, and all4113. CT, C terminus; NT, N terminus.
(C) Sequence alignment of At-PIC1 with its closest relatives from plants (Lj-PIC1; 74% amino acid identity of mature proteins) and cyanobacteria (sll1656 and all4113; 24 and 23% amino acid identity of mature proteins, respectively). Amino acids identical in all four proteins are shown as black-boxed letters, and residues conserved in two or three sequences are shown as gray-boxed letters. The predicted four transmembrane domains of At-PIC1 are boxed, and the potential cleavage site of the chloroplast transit peptide is indicated by a black arrowhead.
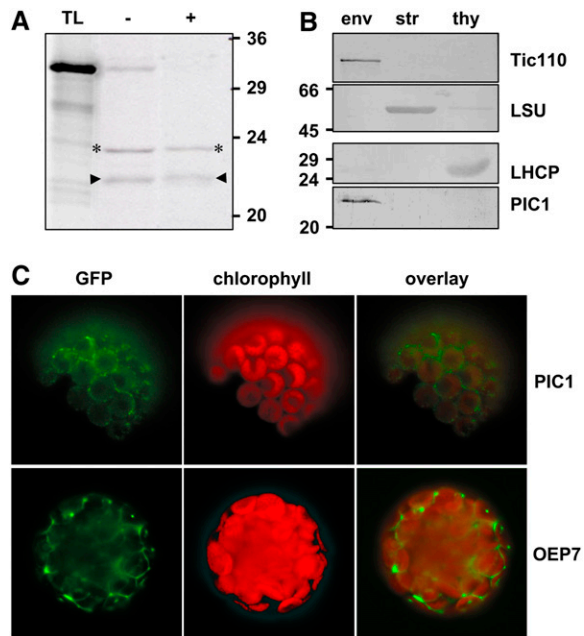
Figure 2. Subcellular Localization of PIC1 to the Inner Envelope of Chloroplasts.

(A) In vitro import of PIC1 into chloroplasts isolated from cotyledons of 8-d-old Col-0 seedlings. Purified intact chloroplasts equivalent to 10 μg of chlorophyll were incubated for 15 min at 25°C with the in vitro–translated 35S-labeled PIC1 precursor protein (TL). After the import reaction, chloroplasts were either not treated (−) or treated (+) with the protease thermolysin for 30 min at 4°C. Intact chloroplasts were recovered by centrifugation, and import products were analyzed by SDS-PAGE and autoradiography. The precursor protein PIC1 is processed to a mature protein of 22 kD (arrowheads). The mature protein as well as an intermediate form of 23.5 kD (asterisks) are protease-protected, confirming import into intact chloroplasts. The translation mixture sample (TL) represents 10% of the precursor added to the import reaction.

(B) Immunoblot analysis of PIC1 localization in chloroplast subfractions. Chloroplasts from 6-week-old *Arabidopsis* rosette leaves were fractionated into envelopes (env), stroma (str), and thylakoid membranes (thy), as described in Methods. Equal amounts of proteins from the subfractions were separated by SDS-PAGE and subjected to immunoblot analysis using an antibody directed against the C-terminal part of At-PIC1. The α-PIC1 stain gave a single band of ~22 kD in chloroplast envelopes only. Antisera against the marker proteins Ps-Tic110 (inner envelope), Ps-LSU (stroma), and Ps-LHCP (thylakoid membranes) were used as controls. Numbers at left indicate the molecular mass of proteins in kilodaltons.

(C) Subcellular localization of PIC1-GFP fusion proteins. *Arabidopsis* mesophyll protoplasts were transiently transformed with constructs for PIC1-GFP and OEP7-GFP. Images are shown for GFP fluorescence, chlorophyll autofluorescence, and an overlay of both. PIC1-GFP signals were localized in a spotted pattern to the periphery of chloroplasts. OEP7-GFP, included as a marker for the chloroplast outer envelope, gave more evenly distributed GFP fluorescence around the chloroplasts.

isolated pea chloroplasts, At-PIC1 displayed the same import pattern (data not shown). All import experiments showed an intermediate product of ~23.5 kD (Figure 2A) that can be pulse-chased into the inner envelope membrane (E. Firlej-Kwoka, personal communication). Thus, we conclude that PIC1 uses the general import pathway into chloroplasts but that insertion into the inner envelope membrane occurs via an intermediate. Based on ChloroP (Emanuelsson et al., 1999), the precursor protein PIC1 of 31.4 kD (296 amino acids) is predicted to have a chloroplast transit peptide with a processing site after amino acid residue 15. However, in vitro import experiments and immunoblot analysis showed a mature protein of ~22 kD (Figures 2A and 2B), requiring the cleavage of a far larger transit peptide. Furthermore, the alignment with all cyanobacterial homologs and the predicted mature proteins of the plant subfamily support this observation (Figure 1A; see Supplemental Figure 1 online). Thus, we conclude that the precursor PIC1 is processed after amino acid residue 81 (Figure 1C), a cleavage site that is supported by ChloroP analysis after removal of the first 15 residues. The resulting mature-sized protein is 216 amino acids long and has a molecular mass of 22.8 kD.

The envelope localization of PIC1 was confirmed by immunoblot analysis. Using antibodies directed against the C-terminal part of PIC1, we detected the mature protein in the envelope fraction of chloroplasts from 6-week-old *Arabidopsis* rosette leaves (Figure 2B). Because the antiserum against PIC1 failed to detect the protein in the entire organelle, chloroplasts were subfractionated into envelopes, stroma, and thylakoid membranes. The mature PIC1 protein runs at an apparent molecular mass of 22 kD. As marker proteins for the chloroplast subfractions, we used antibodies against the chloroplast inner envelope protein Tic110, the large subunit of ribulose-1,5-bis-phosphate carboxylase/oxygenase (LSU), and the thylakoid-bound light-harvesting complex (LHCP) from pea.

To verify the chloroplast localization in intact cells, full-length PIC1 was fused with the green fluorescent protein (GFP) and *Arabidopsis* mesophyll protoplasts were transiently transformed with this construct (Figure 2C). Merging the fluorescence images of GFP and chlorophyll indicated an envelope insertion of PIC1. GFP signals were located at the periphery of chloroplasts only and were associated with neither thylakoid membranes nor cytosolic or plasma membrane components of the cell. However, the GFP distribution appeared more spotted than the even signal of the outer envelope protein At-OEP7 (Lee et al., 2001), which was used as a control. Again, this indicates an association of PIC1 with the inner envelope membrane, because similar GFP signal patterns can be found for the inner membrane–linked VIPP1 (for vesicle-inducing protein in plastids) protein (Aseeva et al., 2004) and the P-type ATPase PAA1 (Abdel-Ghany et al., 2005).

PIC1 Is Ubiquitously Expressed in *Arabidopsis* and Peaks in Green Tissues

When we probed the Affymetrix full genome microarray (ATH1 chip) for the expression of *PIC1* in rosette leaves and roots of 4-week-old *Arabidopsis* (Clausen et al., 2004), it demonstrated that *PIC1* mRNA was present in both tissues but that transcript levels in leaves were approximately twofold higher than those in roots (Figure 3A). This expression pattern could be confirmed by quantitative real-time RT-PCR on cDNA of 7-d-old seedlings (Figure 3B). Here, the relatively high transcript density, 1500 *PIC1* transcripts per 10,000 actin transcripts, originated mostly from cotyledons. Screening the array data of the AtGenExpress
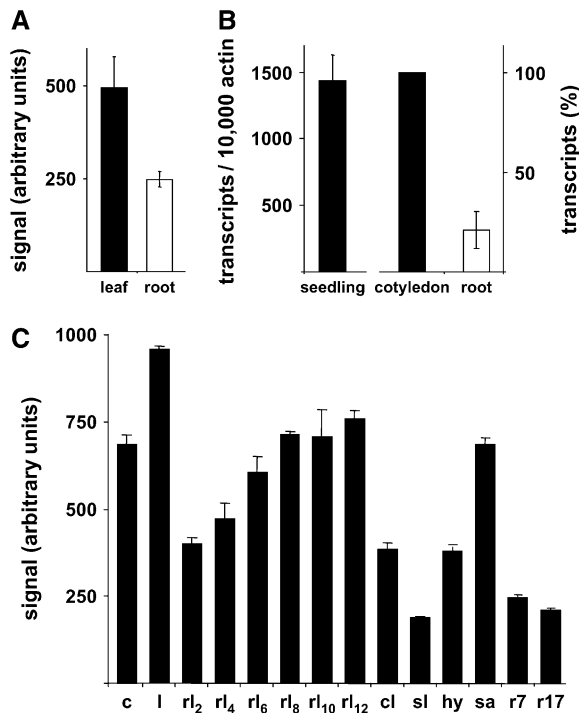
Figure 3. Gene Expression of *PIC1* Peaks in Green Tissues.

(A) Expression profile of *PIC1* in leaves and roots of 4-week-old *Arabidopsis* plants. Microarray signals (Affymetrix GeneChip Arabidopsis ATH1) are made comparable by scaling the average overall signal intensity of all probe sets to a target signal of 100 (arbitrary units). The average scaled signals (±SE) of three independent experiments are shown.

(B) Quantification of *PIC1* mRNA by quantitative real-time RT-PCR in 7-d-old *Arabidopsis* seedlings. Left, the transcript content in whole seedlings is displayed relative to 10,000 transcripts of actin 2/8 ($n = 4$; ±SD). Right, when seedlings were separated into cotyledons and roots, the *PIC1* mRNA in roots was only 21 ± 9% of that in cotyledons. The transcript content was quantified relative to actin 2/8 mRNA ($n = 3$; ±SD) and normalized to the amount in cotyledons, which was set to 100%. Please note that the y axis is divided into two different scales for *PIC1* transcripts/10,000 actin transcripts (left) and *PIC1* transcripts in percentage (right).

(C) In silico transcriptional profiling of *PIC1* expression (arbitrary units) during plant development. Data used to create the in silico transcriptional profiles were obtained from AtGenExpress experiments (Schmid et al., 2005). Signal intensities were averaged from three technical replicates ± SD. c, cotyledons of 7-d-old plants; l, first and second leaves of 7-d-old plants; rl2 to rl12, rosette leaves 2, 4, 6, 8, 10, and 12 of 17-d-old plants; cl, cauline leaves of 21-d-old plants; sl, senescing leaves of 35-d-old plants; hy, hypocotyls of 7-d-old plants; sa, shoot of apex 7-d-old plants; r7, roots of 7-d-old plants; r17, roots of 17-d-old plants.

consortium (Schmid et al., 2005) revealed that *PIC1* is ubiquitously expressed throughout all developmental stages of *Arabidopsis*. Pronounced expression, however, was always linked to green tissues, consistent with a function of the protein in chloroplasts. Whereas mature pollen contained almost no *PIC1* mRNA, the highest transcript content was found in cotyledons and the first two leaves of 7-d-old seedlings, in young rosette leaves, and in the shoot apex (Figure 3C). To further analyze the

gene expression of *PIC1* with respect to abiotic or biotic stimuli, we searched the publicly available databases. However, we did not find *PIC1* to be regulated by any treatment or growth conditions. Moreover, *PIC1* was not regulated by iron-sufficient or -deficient conditions (M.L. Guerinot and E. Rogers, personal communication), nor did it play a role in Zn tolerance (Talke et al., 2006). Thus, it is evident that *PIC1* represents a constitutive and essential gene in *Arabidopsis*.

PIC1 Function Is Essential for Photosynthesis and Plant Growth

In *Arabidopsis*, *PIC1* is encoded by a single-copy gene consisting of four exons (Figure 4A) that are spliced into an mRNA molecule, represented by the National Center for Biotechnology Information reference sequence NM_127089. A promoter prediction analysis suggests a plant TATA box and transcriptional start 206 bp upstream of the translational start, whereas a 3′ untranslated region (UTR) of 186 bp has been annotated for NM_127089. The predicted open reading frame and the length of the 5′ UTR of *PIC1* were verified by RT-PCR analysis on Columbia (Col-0) mRNA.

To understand the function of an ancient permease of cyanobacterial origin in *Arabidopsis* chloroplasts, we characterized three independent T-DNA insertion lines in the *PIC1* gene using PCR genotyping (Figures 4A and 4B; see Methods). By sequencing the respective PCR products between T-DNA and gene-specific primer combinations, we identified T-DNA insertion sites in exon 1 at positions 214 (*pic1-1*) and 320 (*pic1-2*) as well as a mutation in the promoter region (*pic1-3*, position −430). It should be noted that in *pic1-2*, a deletion of 28 bp was found downstream of the insertion site (Figure 4B). As expected, the T-DNA insertions in exon 1 of *pic1-1* and *pic1-2* generated gene knockouts in the homozygous progeny. Whereas primer pairs in 3′ orientation to the T-DNA insertions in *pic1-1* and *pic1-2* detected ~10% residual transcript fragments, no products were amplified when primers were flanking the insertion sites (Figure 4C). By contrast, the mutant allele *pic1-3/pic1-3* contained ~35% residual, fully transcribed *PIC1* mRNA compared with the wild type. Segregation of the mutant alleles was followed in the T3, T4 (for *pic1-1*), T2, and T3 (for *pic1-2* and *pic1-3*) generations. In all plants analyzed, the insertion lines *pic1-1* ($n = 1104$) and *pic1-2* ($n = 270$) split into 20% homozygous and 80% heterozygous/wild-type alleles. The *pic1-3* mutants of the T3 generation segregated in a Mendelian manner.

Whereas the homozygous *pic1-3* and heterozygous *pic1-1* and *pic1-2* mutants showed no obvious phenotype, the appearance of the homozygous, independent knockout alleles *pic1-1* and *pic1-2* was dramatic (Figure 5). The loss of PIC1 function led to dwarfed and chlorotic plants (Figures 5A and 5B). The residual 35% fully transcribed *PIC1* mRNA in homozygous *pic1-3*, however, was sufficient to provide a wild-type appearance to the mutant plants (Figure 5C). Homozygous *pic1-1* and *pic1-2* were seedling-lethal on soil; therefore, heterotrophic growth of the mutants had to be supplemented with 1% sucrose on Murashige and Skoog (MS) agar medium. Cotyledons in young seedlings were red, most likely because chlorophyll was low or absent and anthocyane pigments accumulated (Figure 5A). The majority of
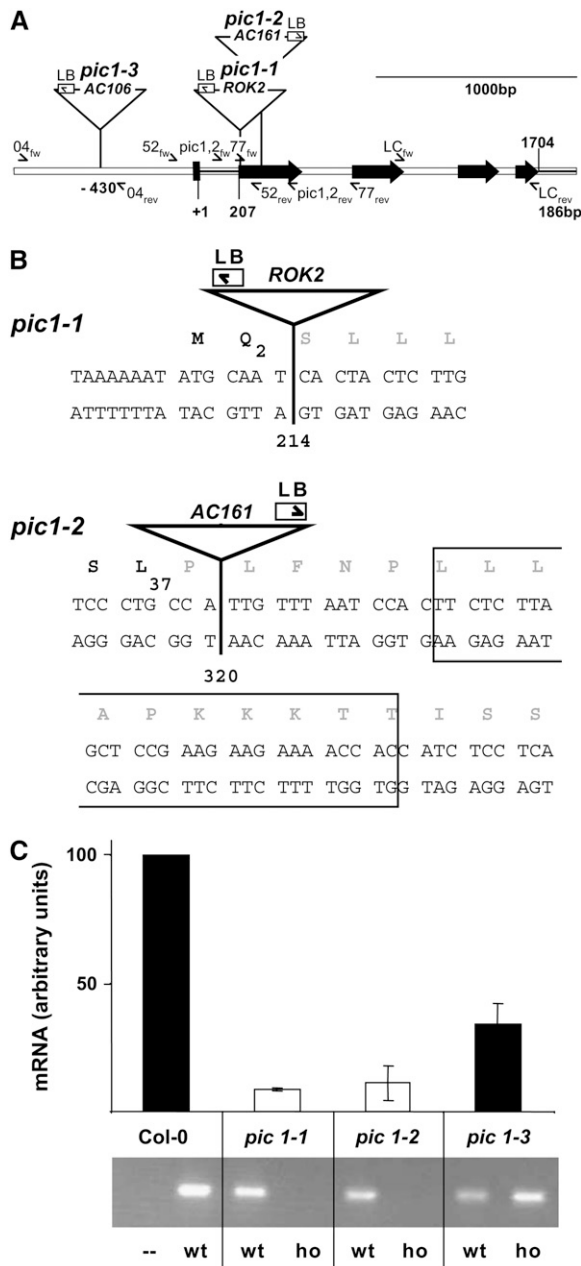
Figure 4. Characterization of *pic1* Mutant Alleles.

(A) Diagram of the genomic organization of *PIC1* and positions of identified T-DNA insertions. The *PIC1* gene is 1704 bp long and comprises four exons (black arrows). The consecutive numbering of the gene starts with the predicted transcriptional start, located behind a potential TATA box (black bar). In consequence, *PIC1* has a 5′ UTR of 206 bp and an annotated 186-bp 3′ UTR (National Center for Biotechnology Information reference sequence NM_127089). In three independent T-DNA insertion lines, the T-DNA has inserted into different parts of exon 1 (*pic1-1* and *pic1-2*) and into the putative promoter region (position −430; *pic1-3*). ROK2, T-DNA present in the SALK collection (SALK_104852); AC161 and AC106, T-DNA present in the GABI-Kat lines 577D06 and 804F07, respectively. Positions and directions of left border T-DNA sequences (LB) and of gene-specific oligonucleotide primers used for PCR geno-

the slowly growing mutants produced almost transparent rosette leaves; however, in approximately one-third of the plants, the leaves appeared white. This subpopulation of mutants was even smaller and did not produce inflorescences (data not shown). Because *pic1-1* and *pic1-2* represent independently derived mutant alleles, the described phenotype in both lines (Figures 5A and 5B) can be linked to the loss of PIC1 function. Roots, like the entire *pic1* mutant plant, were smaller than in wild-type plants. However, we did not observe any significant phenotype in roots of *pic1* mutants maintained on sucrose-supplemented medium.

To complement the mutant phenotype, a 3327-bp genomic fragment containing the *PIC1* gene and the promoter region (*gPIC1*) was introduced into heterozygous *PIC1/pic1-1* plants. Six independent T1 lines that inherited the *gPIC1* construct were generated. According to segregation analysis of the *PIC1* locus by PCR genotyping in the T1 and T2 generations, one of these lines proved to be homozygous for the *pic1-1* allele (*pic1-1/pic1-1 gPIC1-1*), four lines were still heterozygous (*PIC1/pic1-1 gPIC1-2, -3, -4,* and *-5*), and one line was wild type (*PIC1/PIC1 gPIC1-6*) at the endogenous *PIC1* locus. The line *pic1-1/pic1-1 gPIC1-1* had deep green leaves and showed normal development in the T1 and T2 generations (Figure 5A), proving the complementation of the homozygous *pic1-1* mutant by *gPIC1-1*.

Interestingly, the shoot apex and the very young emerging leaves of homozygous *pic1-1* and *pic1-2* mutants were pale green and their leaves turned chlorotic while growing (Figure 5D). After 6 weeks on sucrose-containing agar, surviving mutant plants were able to produce an inflorescence; again, the young sepals of the flower were pale green and became white subsequently

typing of *pic1* mutants (04fw, 04rev, 52fw, 52rev, 77fw, and 77rev) and for RT-PCR (pic1,2fw, pic1,2rev, LCfw, and LCrev) are depicted.

(B) The T-DNA in *pic1-1* and *pic1-2* interrupts the open reading frame of *PIC1*. In *pic1-1*, the T-DNA *ROK2* has inserted at position 214 of the *PIC1* gene, interrupting the open reading frame behind amino acid 2. In *pic1-2*, the *AC161* T-DNA blocks translation after amino acid 37 of exon 1 (position 320 of *PIC1*). Please note that behind the T-DNA insertion site, we identified a deletion of 28 bp (boxed letters) in the *PIC1* coding region.

(C) Homozygous mutations in *pic1-1* and *pic1-2* result in loss of full-length *PIC1* transcripts. Top graph, quantification of *PIC1* transcripts in 7-d-old seedlings of Col-0 wild type and homozygous *pic1-1*, *pic1-2*, and *pic1-3* mutant lines. Transcript density was measured by quantitative real-time RT-PCR with the primer pair LCfw-rev (see **[A]**) as described in Methods. The *PIC1* mRNA content ($n = 3$; $\pm$SD) was calculated relative to actin 2/8 transcripts and normalized to the amount in Col-0 seedlings, which was set to 100% (arbitrary units). Whereas in *pic1-1/pic1-1* and *pic1-2/pic1-2* the mRNA level was ∼10% of wild-type RNA (white bars), *pic1-3/pic1-3* seedlings contained 34 ± 8.4% of Col-0 *PIC1* mRNA (black bars). Bottom panel, RT-PCR experiments with pic1,2fw-rev primers (see **[A]**), which flank the T-DNA insertion sites of *pic1-1* and *pic1-2* mutant alleles. PCR was performed on cDNA of 7-d-old seedlings from Col-0 as well as from homozygous *pic1-1*, *pic1-2*, and *pic1-3* (ho) and the corresponding wild-type alleles *PIC1-1/PIC1-1*, *PIC1-2/PIC1-2*, and *PIC1-3/PIC1-3* (wt). Please note that the primer pair pic1,2fw-rev was not able to amplify a specific product (343 bp) on homozygous *pic1-1* and *pic1-2* mutants, indicating that these alleles lack full-length PIC1 transcripts. In turn, the 10% residual RNA detected by quantitative RT-PCR with C-terminal primers (top graph) most likely resulted from incomplete mRNA.
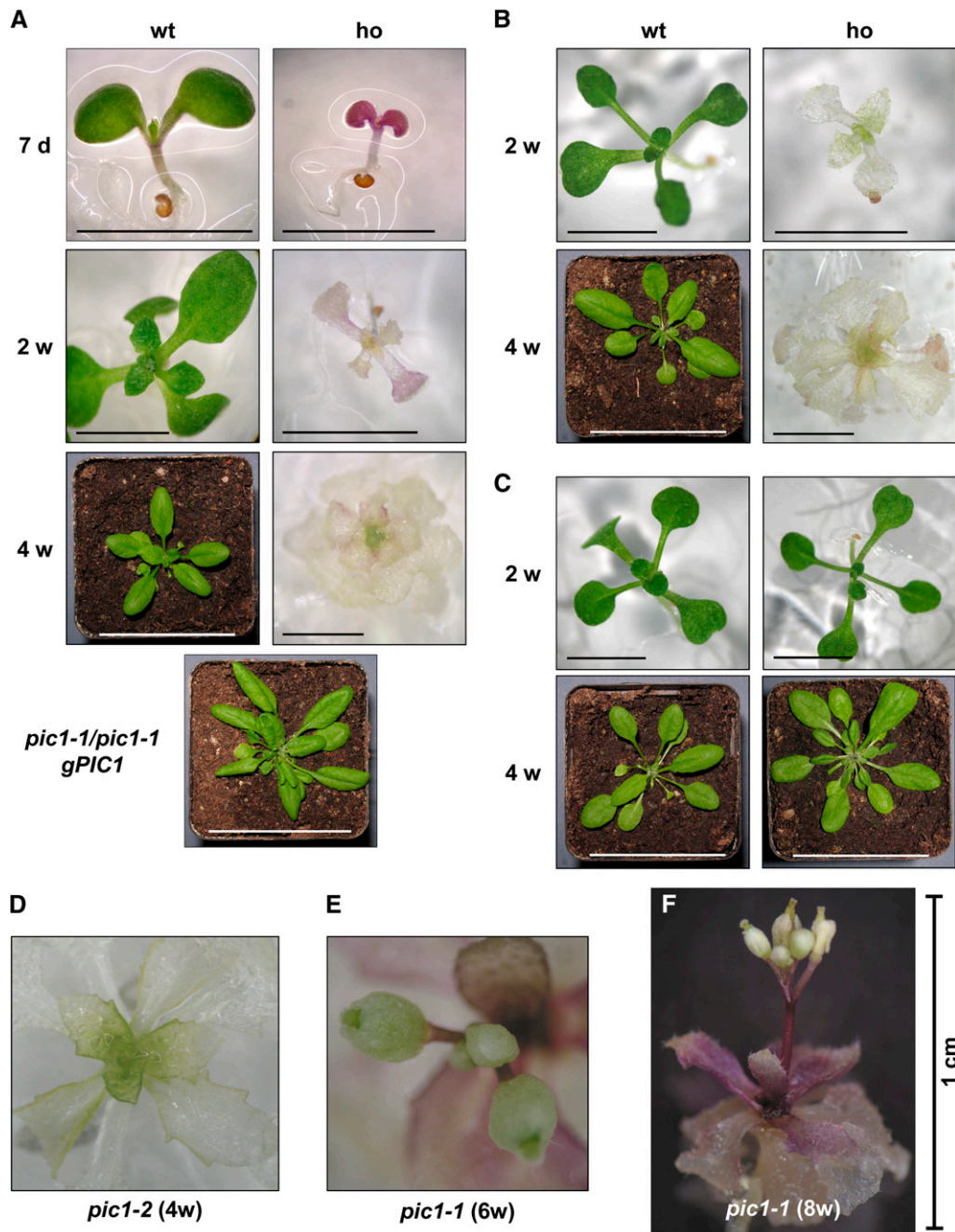
Figure 5. Loss of PIC1 Generates Chlorotic and Dwarfed Mutant Plants.

The phenotypes of homozygous *pic1* mutants (ho) and the corresponding wild-type alleles (wt) are depicted. The age of the plants is given in days (d) or weeks (w). Homozygous plants of *pic1-1* and *pic1-2* mutants were grown on MS agar medium supplemented with 1% sucrose. If not indicated otherwise, black bars = 0.5 cm and white bars = 5.0 cm.

(A) Homozygous *pic1-1* mutants are dwarfed and chlorotic. Cotyledons in 7-d-old seedlings of homozygous *pic1-1/pic1-1* (ho) are red. The first leaves after 2 weeks are transparent, and so is the fully grown rosette in the dwarfed plants after 4 weeks of growth. Please note that the shoot meristem of *pic1-1/pic1-1* is pale green (cf. **[B]** and **[D]**). In *pic1-1/pic1-1 gPIC1* (T2 generation, 4 weeks old), the loss of PIC1 has been fully complemented by transformation of the mutant with the *PIC1* gene (see Methods).

(B) *pic1-2/pic1-2* plants display the same phenotype described for *pic1-1/pic1-1* in **(A)**.

(C) The residual 35% of fully transcribed *PIC1* mRNA in homozygous *pic1-3* mutants (see Figure 3C) is enough to produce mutant plants with wild-type appearance.

(D) Close-up of shoot apex and young leaves of a homozygous *pic1-2* mutant plant (4 weeks old). Meristem and young leaves of the mutant are pale green, whereas older leaves become chlorotic during development and growth.

(E) Close-up of developing inflorescence of a homozygous *pic1-1* mutant plant (6 weeks old). Young sepals and the style of the flower are pale green.

(F) Fully developed homozygous *pic1-1* mutant after 8 weeks of growth. The sepals of the flower have turned white, the styles and developing siliques are pale green, and the rosette leaves and the stem of the plant are red.

(Figure 5E). Eight-week-old plants were fully grown with a mature size of 1 cm. The style and developing silique of the flower were pale green, whereas leaves and stem accumulated anthocyane pigments (Figure 5F). Because all flowers of homozygous mutants were sterile, *pic1-1* and *pic1-2* had to be propagated in the heterozygous state.

In summary, the described phenotypes of *pic1-1* and *pic1-2* mutants suggest an essential function of PIC1 in photosynthesis and plant growth. Obviously, loss of PIC1 function produces chlorotic plants, which are not able to assimilate carbohydrates by photosynthesis. Hence, their growth has to be supplemented with sucrose.

Loss of PIC1 Function Leads to Impaired Chloroplast Development

Next, leaf morphology and ultrastructure were analyzed in the homozygous *pic1-1* mutant. Compared with Col-0 wild type (Figure 6A), mature rosette leaves of *pic1-1* were retarded in growth (Figure 6B). Interestingly, secondary and tertiary veins in *pic1-1* leaves were thicker than in the wild type, and their diameter was commensurate with that of the primary vein. The organization of leaf mesophyll into palisade and spongy parenchyma cells was lost in *pic1-1/pic1-1*, and the leaf surface was extremely curled (Figures 6C to 6F). This deformation in the mutant leaf was already visible in cotyledons (Figure 6F). In addition, leaf cross sections revealed that mesophyll cells of homozygous *pic1-1* (Figures 6D, 6F, and 6H), in contrast with wild-type plants (Figures 6C, 6E, and 6G), do not contain fully differentiated chloroplasts. Thus, the chlorotic phenotype of *pic1-1/pic1-1* plants results from impaired chloroplast development.

To further follow chloroplast development in the mutant *pic1-1/pic1-1*, the ultrastructure of chloroplasts in 7-d-old cotyledons as well as in rosette leaves and the shoot apex of 17-d-old plants was investigated by transmission electron microscopy (Figure 7). In general, compared with the wild type (Figures 7A and 7D), mutant plastids in cotyledons and leaves were reduced in size and number. Moreover, the development of thylakoids was extremely disturbed in mutant plastids. In mutant cotyledons, two types of plastids were present: (1) a proplastid-like stage, in which rudimentary thylakoids were present (Figure 7B), and (2) a stage in which thylakoids were absent (Figure 7C). In addition, plastids of various stages of degradation were observed in the cytoplasm or in fusion with vacuoles (data not shown). The degeneration of thylakoids was even more pronounced in rosette leaves of *pic1-1* (Figures 7E and 7F). Here, we found plastids characterized by the formation of membrane vesicles of various sizes in the stroma and plastids without thylakoids. Proplastid-like organelles, as typical for cotyledons or the shoot apex (see below), did not exist in *pic1-1* leaves. In the shoot apical meristem of wild-type plants (Figure 7G), formation of thylakoids was observed in developing chloroplasts. By contrast, in *pic1-1*, early developmental stages of chloroplasts were present next to plastids without any thylakoids in the same cell (Figure 7H). Furthermore, plastids without thylakoids possessed an electron-translucent matrix. Thus, the loss of PIC1 leads to a dramatic distortion in chloroplast development, characterized by inchoate or absent thylakoids.
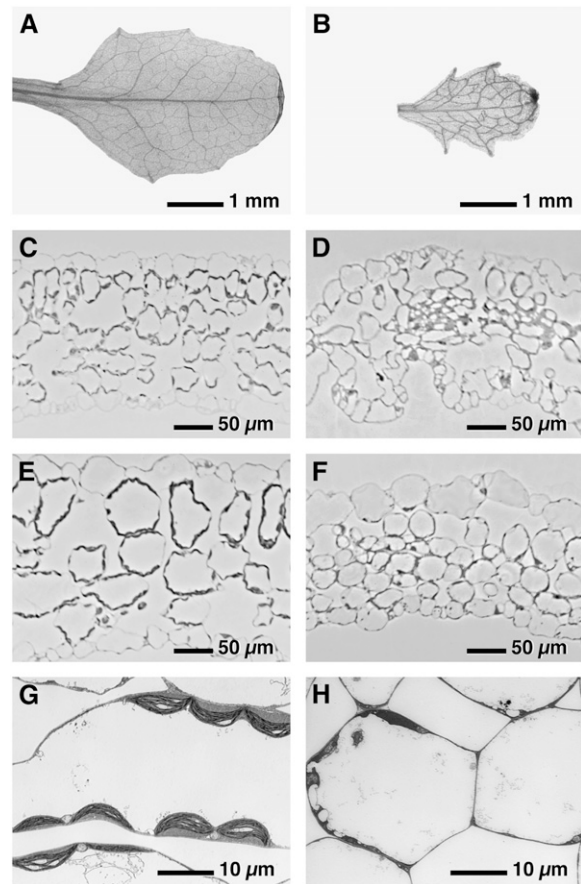
Figure 6. Leaf Morphology Is Changed in *pic1-1* Mutant Plants.

(A) and **(B)** Rosette leaves from 4-week-old Col-0 wild-type **(A)** and homozygous *pic1-1* mutant **(B)** plants. Leaves of *pic1-1/pic1-1* are reduced in size, and the diameter of primary, secondary, and tertiary veins is not graduated, as in the wild type. Before photography, leaves were destained in 70% ethanol.

(C) to **(F)** Semithin cross sections of rosette leaves from 17-d-old Col-0 wild-type **(C)** and *pic1-1/pic1-1* **(D)** as well as from 7-d-old cotyledons of Col-0 **(E)** and homozygous *pic1-1* **(F)**. In *pic1-1/pic1-1* mutants, the organization of the leaf mesophyll into palisade and spongy parenchyma cells is lost **(D)**. Furthermore, the leaf surface is extremely curled, and inside the cells no chloroplasts are visible (**[D]** and **[F]**).

(G) and **(H)** Transmission electron micrographs of cortex cells from 7-d-old cotyledons of Col-0 **(G)** and *pic1-1/pic1-1* **(H)** seedlings. Please note that the cotyledon cells in homozygous *pic1-1* plants do not contain correctly developed chloroplasts **(H)**.

Loss of PIC1 Affects Metal Homeostasis in Plastids and in the Cytosol

Surprisingly, plastids in the mutant plants were characterized by the presence of phytoferritin aggregates (Figures 7H and 7I) (see Hirsch et al. [2006] for ferritin in *Arabidopsis* chloroplasts). The electron-dense ferritin clusters were detected in plastids of cotyledons, leaves, and shoot apices of *pic1-1/pic1-1* but not in any chloroplasts of wild-type plants (Figures 7A, 7D, and 7G). When we compared gene expression in *pic1-1* versus the wild
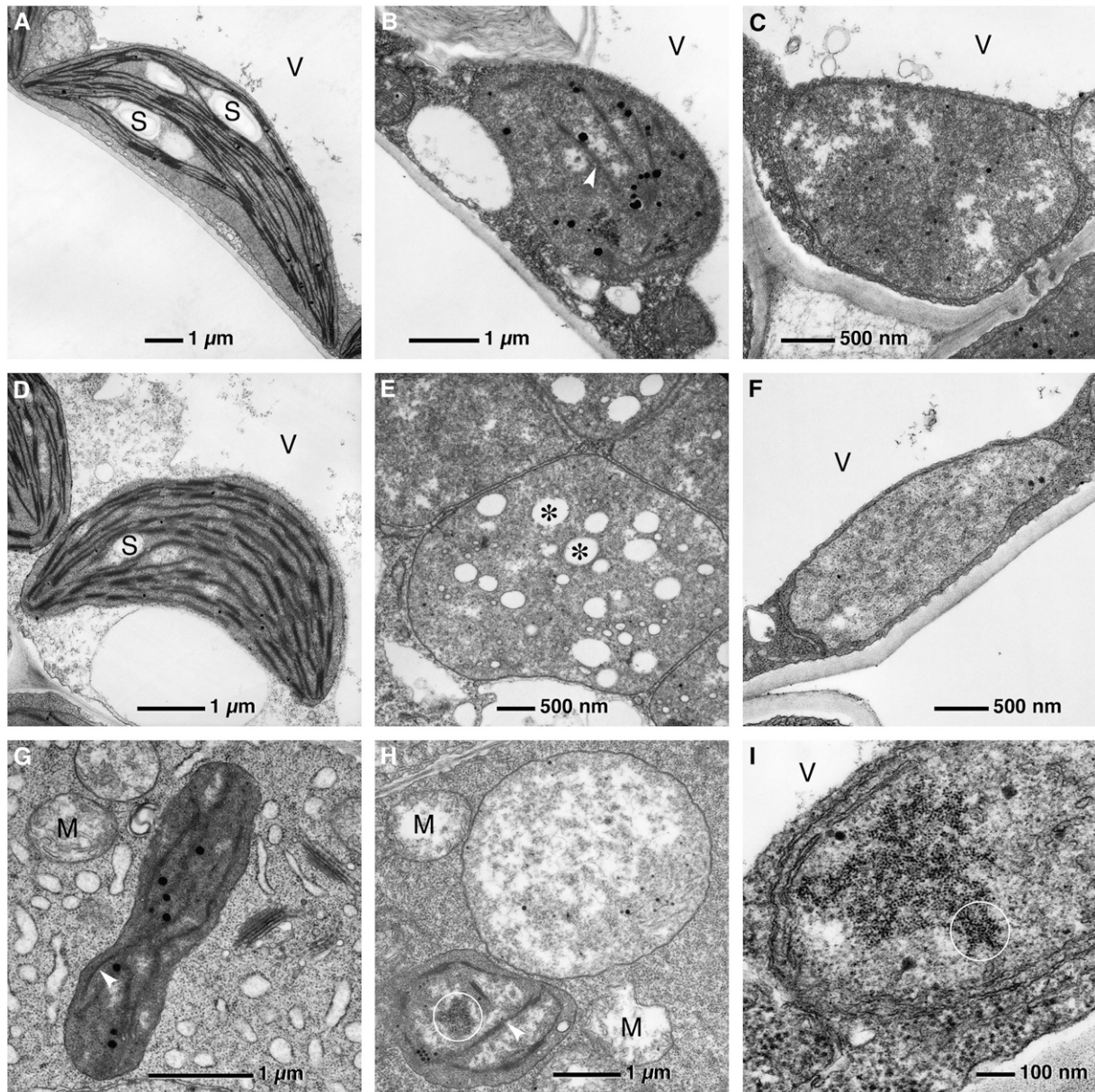
Figure 7. Chloroplast Development in *pic1-1/pic1-1* Is Impaired, and Mutant Plastids Accumulate Ferritin.

Chloroplast ultrastructure was monitored by transmission electron microscopy. Plastoglobules were present in plastids of mutant and wild-type plants at all developmental stages. M, mitochondria; S, starch grains; V, vacuoles.

(A) to **(C)** Plastids from 7-d-old cotyledons. **(A)** shows a control chloroplast (Col-0 wild type) containing grana and stroma thylakoids, starch grains, and plastoglobules. By contrast, plastids of the mutant *pic1-1/pic1-1* are about half the size and contain only inchoate (**[B]**, white arrowhead) or no **(C)** thylakoids.

(D) to **(F)** Chloroplasts in 17-d-old rosette leaves of Col-0 **(D)** and *pic1-1/pic1-1* (**[E]** and **[F]**). Two types of plastids were present in rosette leaves of homozygous *pic1-1*: plastids characterized by the formation of membrane vesicles (asterisks) in the stroma **(E)**, and plastids without thylakoids **(F)**.

(G) and **(H)** Proplastids in the shoot apex of 17-d-old plants. In the differentiating meristem of Col-0 wild-type plants **(G)**, proplastids were characterized by developing thylakoid systems (white arrowhead). The shoot apex of *pic1-1/pic1-1* **(H)** contains proplastids with developing thylakoids (white arrowhead) as well as without thylakoids and less electron-dense matrix (organelle at top right) in the same cell. In *pic1-1* mutant plastids, phytoferritin clusters (white circles) are visible.

(I) Ferritin cluster typical for plastids of cotyledons from 7-d-old *pic1-1/pic1-1*.

type by Affymetrix microarray analysis (SAM software; Tusher et al., 2001), an increase of transcripts for *FER1* and *FER4* in *pic1-1/pic1-1* mutants was found (Table 1). Furthermore, ferritin protein accumulated in homozygous *pic1-1* and *pic1-2* mutants but was not detectable in wild-type leaves (Figure 8A). Because all ferritin detected in the mutants was processed to the mature size of 23.5 kD, it is evident that it is plastid-intrinsic (Figures 7H and 7I). No ferritin precursor protein (28 kD) was detected. In conclusion, *pic1* mutant plants increased the levels of ferritin transcripts and protein, leading to the formation of ferritin clusters within plastids. Because ferritin in plants has been described as a storage protein for iron in plastids (Briat and Lobreaux, 1997), the loss of PIC1 function might interfere with iron homeostasis in mutant plastids.

In addition to ferritin, we found the transcripts of the copper superoxide dismutases CSD1 and CSD2 to be upregulated in *pic1-1/pic1-1* (Table 1). Again, the transcriptional regulation could be verified by immunoblot analysis, in which specific antibodies for CSD1 and CSD2 detected the proteins in homozygous *pic1-1* and *pic1-2* mutants only (Figure 8A). Whereas CSD1 is localized in the cytosol, CSD2 is plastid-intrinsic (Kliebenstein et al., 1998). The increase of both CSD proteins in the cytosol and in plastids was accompanied by a twofold increase of the Cu content in *pic1-1* shoot tissue (see Supplemental Table 1 online). Thus, metal ion homeostasis was affected not only in plastids but also within the cytosol of *pic1* mutants. By contrast, transcripts and protein levels of the plastid-localized, Fe-dependent superoxide dismutase FSD1 (Kliebenstein et al., 1998) were slightly downregulated (Table 1, Figure 8A).

Photosynthetic Capacity Is Lost but Protein Import Is Still Functional in *pic1* Plastids

Whereas metal homeostasis–associated proteins in *pic1* mutants are differentially regulated, the photosynthetic capacity of mutant plastids was completely lost. This becomes apparent by the heterotrophic growth and chlorosis of homozygous *pic1-1* and *pic1-2* (Figures 5 and 6), the impaired biogenesis and degradation of thylakoids (Figure 7), and the downregulation of genes associated with photosynthesis and carbon assimilation

Table 1. Differential Expression of Genes Related to Iron Homeostasis, Metal Transport, and Photosynthesis in Homozygous *pic1-1* versus Wild-Type Plants

Gene	AGI Code	Signal, *pic1-1*	Signal, Wild Type	Change Direction	Fold Change	P Value	Subcellular Localization
Iron homeostasis							
FER1	At5g01600	1573 ± 188	632 ± 192	Up	2.49	0.022889247	C (S)
FER4	At2g40300	304 ± 41	113 ± 33	Up	2.68	0.019333906	C (S)
CSD1	At1g08830	1921 ± 87	572 ± 111	Up	3.36	0.004239178	cyt
CSD2	At2g28190	1614 ± 205	454 ± 106	Up	3.55	0.016714474	C (S)
FSD1	At4g25100	1209 ± 293	2574 ± 534	Down	0.47	0.053113348	C (S)
Metal transport							
GCN1	At5g60790	328 ± 56	209 ± 33	Up	1.57	0.045228228	cTp
NRAMP1	At1g80830	337 ± 31	223 ± 31	Up	1.51	0.029790649	cTp
NRAMP6	At1g15960	47 ± 5.7	25 ± 6	Up	1.89	0.029790649	cTp
YSL1	At4g24120	150 ± 42	27 ± 12	Up	5.64	0.027014065	?
IRT1	At4g19690	5.7 ± 1.4	28 ± 7.2	Down	0.20	0.029790649	PM
PAA1	At4g33520	101 ± 22	185 ± 18	Down	0.54	0.029790649	C (IE)
COPT2	At3g46900	32 ± 9	199 ± 33	Down	0.16	0.01693783	?
Photosynthesis							
LHCB4.1	At5g01530	1524 ± 102	3929 ± 165	Down	0.39	0	C (T)
LHCB4.2	At3g08940	921 ± 105	3954 ± 247	Down	0.23	0	C (T)
LHCB4.3	At2g40100	56 ± 10	379 ± 62	Down	0.15	0.01693783	C (T)
PSBO-1	At5g66570	2000 ± 226	4232 ± 344	Down	0.47	0.016845739	C (T)
PORB	At4g27440	117 ± 35	239 ± 38	Down	0.49	0.045228228	C (S)
PORC	At1g03630	182 ± 39	828 ± 120	Down	0.22	0.01693783	C (S)
RBCS-1A	At1g67090	3855 ± 128	7420 ± 442	Down	0.52	0.006030996	C (S)
Housekeeping							
SerRS	At5g27470	582 ± 55	572 ± 85	No			C (S)
NDPK	At5g63310	765 ± 127	932 ± 89	No			C (S)
Toc 75-III	At3g46740	246 ± 19	184 ± 91	No			C (OE)
OEP16.1	At2g28900	218 ± 35	326 ± 88	No			C (OE)

Signal values for genes with housekeeping functions in chloroplasts are shown for comparison. Affymetrix ATH1 microarry analysis was performed on 14-d-old seedlings of *pic1-1* mutant and Col-0 wild-type plants as described in Methods. The average scaled signals ($n = 3$; ±SD) are depicted. Signal differences were evaluated by SAM software (Tusher et al., 2001), resulting in change direction, fold change, and corresponding significance measures (P value, false discovery rate = 5.31%). For details of the analysis, see Methods and Supplemental Table 2 online. Please note that housekeeping genes in the chloroplast are not differentially expressed (no change). The Arabidopsis Genome Initiative (AGI) code for each gene is given, and the subcellular localization of the corresponding protein is designated as follows: C, chloroplast; cTP, predicted chloroplast transit peptide; cyt, cytosol; IE, inner envelope; OE, outer envelope; PM, plasma membrane; S, stroma; T, thylakoids; ?, unknown.
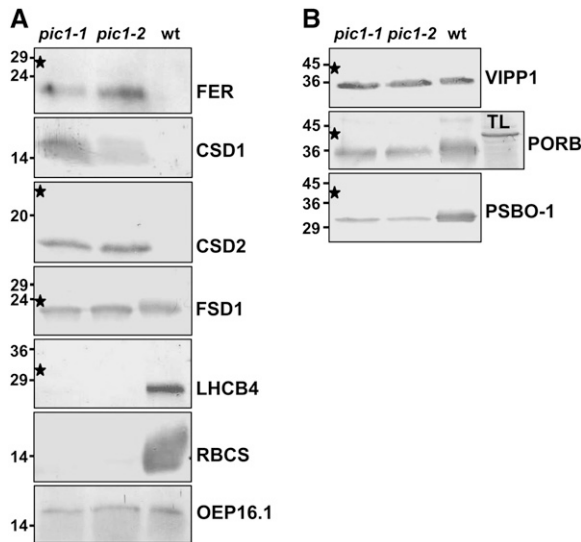
Figure 8. Immunoblot Analysis of *pic1* Mutants and Wild-Type Plants.

Fifty micrograms of total protein, extracted from leaves of 4-week-old homozygous *pic1-1* and *pic1-2* mutants and Col-0 wild-type plants, were subjected to immunoblot analysis. Numbers at left indicate the molecular mass in kilodaltons, and asterisks indicate the molecular mass of the respective precursor proteins. Except for RBCS (tobacco [*Nicotiana tabacum*]), VIPP1 (pea), and PSBO-1 (spinach [*Spinacia oleracea*]), all antisera are directed against *Arabidopsis* proteins. Below, the molecular mass in kilodaltons of the respective precursor (pre) and mature (mat) forms of all proteins is indicated, and the chloroplast localization is specified. For Arabidopsis Genome Initiative codes of *Arabidopsis* proteins, see Table 1.
(A) Proteins related to metal homeostasis are differentially regulated, whereas proteins associated with photosynthesis and carbon fixation are absent in *pic1* mutants. Antisera against the following proteins were used: FER (ferritin; 28 pre, 23.5 mat, stroma), CSD1 (cytosolic copper superoxide dismutase; 15 kD), CSD2 (plastidic CSD; 22 pre, 18 mat, stroma), FSD1 (plastidic iron superoxide dismutase; 24 pre, 23 mat, stroma), LHCB4 (chlorophyll binding protein B4; 31 pre, 27 mat, attached to thylakoids), RBCS (small subunit of ribulose-1,5-bis-phosphate carboxylase/oxygenase; 20.2 pre, 14 mat, stroma), and OEP16.1 (outer envelope protein in chloroplasts of 16 kD). Please note that the FER antibody detects the ferritin protein family in *Arabidopsis* (FER1 to FER4) and LHCB4 reacts with the proteins LHCB4.1, -4.2, and -4.3 (see Table 1).
(B) Chloroplast-localized proteins are properly imported into *pic1* mutant plastids and processed to their mature size. Antisera against the following proteins were used: VIPP1 (vesicle-inducing protein in plastids; 43 pre, 36 mat, inner envelope), PORB (protochlorophyllide oxidoreductase B; 43 pre, 36 mat, stroma), and PSBO-1 (33-kD subunit of the oxygen-evolving complex; 40.5 pre, 33 mat, thylakoid lumen). TL, in vitro translation product of the precursor PORB. Please note that the PORB antibody detects PORB and PORC, both of which are decreased in *pic1* mutant leaves (see Table1).

(Table 1). For example, transcript abundance of chlorophyll binding proteins (e.g., LHCB4), subunits of the oxygen evolving complex (e.g., PSBO-1), proteins involved in chlorophyll biosynthesis (e.g., protochlorophyllide oxidoreductase; POR), and ribulose-1,5-bis-phosphate carboxylase/oxygenase (e.g., RBCS-1A) was decreased dramatically in *pic1* mutants. Again, we verified these data by immunoblot analysis, in which LHCB4 and

RBCS-1A proteins were not detectable and POR as well as PSBO-1 were decreased in *pic1* mutants compared with the wild type (Figures 8A and 8B). It should be noted that all detected plastid-localized proteins were processed to their mature form in *pic1* mutants (i.e., imported into the mutant plastids).

To further analyze the protein import capacity of *pic1* mutant plastids, we chose the following proteins: VIPP1, which is localized at the inner chloroplast envelope (Aseeva et al., 2004); POR, which is localized in the chloroplast stroma; and PSBO-1, which is localized in the thylakoid lumen (Figure 8B). All three proteins were imported into plastids and processed to their mature size, as shown by immunoblot analysis. We never detected any residual precursor proteins in *pic1* mutants, indicating that protein import into plastids is functional in *pic1*.

In contrast with proteins linked to metal homeostasis or photosynthesis, genes associated with housekeeping functions in the chloroplast stroma, such as aminoacyl tRNA synthetases (e.g., *SerRS*) or a nucleoside-diphosphate kinase (*NDPK*), as well as the general protein import pore Toc75 (*Toc 75-III*) and the amino acid–selective channel OEP16 (*OEP16.1*) in the outer chloroplast envelope, were not regulated in *pic1* mutants (Table 1, Figure 8A).

PIC1 and Its Homolog from *Synechocystis* Mediate Iron Uptake in Yeast

Several cyanobacterial relatives of At-PIC1 are annotated as potential permeases for metal ions. In addition, the upregulation of ferritin gene expression and the accumulation of ferritin proteins in homozygous *pic1-1* and *pic1-2* mutants suggest a possible function of PIC1 in iron transport into chloroplasts. Furthermore, the phenotype of *pic1* mutants, in particular leaf chlorosis, inhibition of chloroplast development, and lack of palisade parenchyma differentiation, is reminiscent of iron deficiency (Henriques et al., 2002; Varotto et al., 2002).

To investigate a potential role of PIC1 in metal transport across the plastidic inner envelope, we expressed the cDNA of *PIC1* and its cyanobacterial homolog *sll1656* from *Synechocystis* in the yeast double mutant *fet3 fet4*, which is defective in low- and high-affinity Fe uptake (Dix et al., 1994). Because of its reliance on additional and less efficient uptake mechanisms, the *fet3 fet4* mutant requires high Fe concentrations in its growth medium. *PIC1* and *sll1656* cDNAs in the yeast expression vector pFL61 were transformed into *fet3 fet4* yeast mutants. The cDNA of the iron transporter IRT1 from *Arabidopsis* roots (Eide et al., 1996) and the empty vector pFL61 were used as positive and negative controls, respectively. Because the *fet3 fet4* mutant cannot grow under iron-limited conditions, the ability of the transformants to grow on minimal medium supplemented with Fe concentrations ranging from 0 to 20 μM FeCl$_3$ was investigated (Figure 9A). Whereas yeast cells expressing the empty vector did not grow on 5 μM FeCl$_3$, expression of the Fe^{2+} transporter gene *IRT1* from *Arabidopsis* efficiently complemented yeast growth. Expression of *PIC1* and *sll1656* restored the ability of *fet3 fet4* to grow when supplemented with 5 μM or greater concentrations of FeCl$_3$. Similarly, in liquid minimal medium containing 20 μM FeCl$_3$, *fet3 fet4* mutant cells expressing either *PIC1* or *sll1656* entered the exponential growth phase 2 to 3 h earlier than the vector control
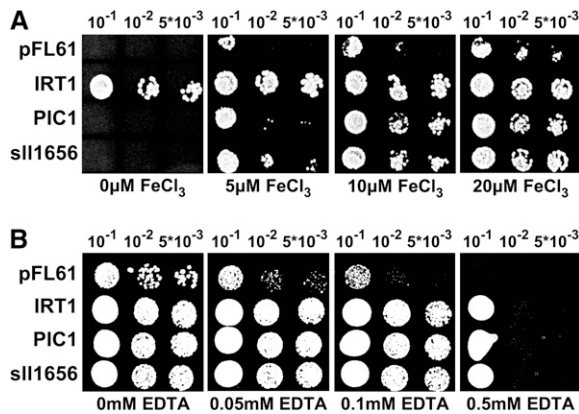
Figure 9. PIC1 and Its *Synechocystis* Homolog sll1656 Are Able to Complement the Growth of Metal Uptake–Defective Yeast Mutants.

The plasmid pFL61 (empty vector control) as well as the cDNA of IRT1, PIC1, and sll1656 in pFL61 were introduced into the *fet3 fet4* **(A)** and *ctr1* **(B)** yeast mutants. Serial dilutions with an OD_{600} of 10^{-1}, 10^{-2}, and 5×10^{-3} of rapidly growing yeast cells were dotted on SC (−uracil) minimal medium, pH 5.0, supplemented with different concentrations of $FeCl_3$ or EDTA as indicated. The growth of yeast cells was documented after 2 d on the plate.

(A) PIC1 and sll1656 are able to restore the growth of *fet3 fet4* in the concentration range 5 to 10 μM $FeCl_3$. IRT1-complemented *fet3 fet4* cells are able to grow without additional iron, whereas dilutions of the empty vector–containing cells (pFL61) need 20 μM $FeCl_3$ to grow.

(B) With 0.1 and 0.5 mM EDTA in the medium, PIC1, sll1656, and IRT1 are still able to restore the growth of the yeast mutant *ctr1*. By contrast, cells transfected with the empty vector pFL61 grow poorly on 0.1 mM EDTA and fail to grow with 0.5 mM EDTA in the medium.

(data not shown). However, the complementation was not as efficient as with *IRT1*.

In addition, we determined whether *PIC1* and *sll1656* could complement the *ctr1* mutant, which is defective in Cu transport (Dancis et al., 1994a). The *ctr1* mutant cannot grow on copper-limiting medium or on medium containing EDTA (Dancis et al., 1994b; Korshunova et al., 1999). Expression of *PIC1*, *sll1656*, and *IRT1* in the *ctr1* mutant strain did rescue its growth defect on medium with concentrations of EDTA of >0.05 mM, whereas cells transformed with the pFL61 vector control grew poorly (Figure 9B). However, because of the Cu dependence of Fe uptake in yeast (Dancis et al., 1994b), we cannot distinguish whether the growth complementation of *ctr1* in this experiment is the result of restored copper or iron uptake.

To show whether complementation of the *fet3 fet4* mutant by PIC1 and sll1656 is attributable to iron uptake into the cells, we measured short-term ^{59}Fe accumulation in *fet3 fet4* cells transformed with the empty vector pDR195 or the cDNAs of IRT1 (positive control), PIC1, and sll1656 in pDR195 (Table 2). The expression of either protein, PIC1 or sll1656, significantly increased the Fe uptake rates compared with the vector control. In agreement, with the growth complementation assays, however, Fe uptake rates mediated by PIC1 and sll1656 were severalfold lower than those mediated by IRT1. These results support a direct role of these two proteins in the membrane transport of iron.

DISCUSSION

PIC1, an Ancient Permease in the Inner Envelope of Plastids

The protein PIC1 contains four predicted transmembrane α-helices and is integral to the inner envelope of *Arabidopsis* chloroplasts. The chloroplast membrane localization of PIC1 was already indicated by proteome analysis (Froehlich et al., 2003). We showed here the insertion of PIC1 into the *Arabidopsis* chloroplast envelope by immunoblot analysis, by in vitro protein import experiments, and by in vivo GFP labeling of the protein (Figure 2). Immunoblot and GFP analyses clearly excluded a thylakoid membrane localization, and processing of the imported precursor protein PIC1 suggested an integration into the inner rather than the outer chloroplast envelope. In summary, the results demonstrate an inner envelope localization of PIC1. The PIC1 homolog sll1656 in *Synechocystis* most likely is integral to the plasma membrane of the cyanobacterium.

Sequence comparison revealed that besides the PIC1 family in vascular plants and green and red algae, the only relatives of PIC1 are of cyanobacterial origin. Thus, it is very likely that PIC1 proteins evolved directly during endosymbiosis between a cyanobacterium and an ancient eukaryotic cell. This evolutionary step led to the formation of chloroplasts and hence to their function in photosynthesis in land plants and algae (Vothknecht and Soll, 2005). Because of the severe phenotype of *pic1* knockout plants, it became evident that PIC1 function is essential for thylakoid biogenesis and, in turn, for photosynthesis. The fact that the cyanobacterium *G. violaceus* contains neither thylakoid membranes (Nakamura et al., 2003) nor PIC1 homologs emphasizes this observation.

PIC1 proteins of cyanobacterial origin belong to COGs (Tatusov et al., 2003), which generally play a role in ion or solute transport across membranes. Several cyanobacterial relatives of PIC1 have been annotated as potential permease components of ABC transporters. Unlike eukaryotic ABC transporters,

Table 2. Iron Uptake in Yeast Is Mediated by PIC1 and Its *Synechocystis* Homolog sll1656

Sample	Fe Accumulation	Fold Increase	P Value	SNK Test
pDR195	104.61 ± 8.93			c
IRT1	869.02 ± 29.94	8.3 ± 0.29	P < 0.001	a
PIC1	153.11 ± 12.85	1.5 ± 0.12	P = 0.020	b
sll1656	141.29 ± 1.92	1.4 ± 0.02	P = 0.030	b

The plasmid pDR195 (empty vector control) as well as the cDNA of IRT1, PIC1, and sll1656 in pDR195 were introduced into *fet3 fet4* yeast mutants. After growth to the exponential phase, yeast cultures were assayed for ^{59}Fe uptake as described in Methods. Fe accumulation (pmol Fe/10^6 yeast cells ± SD) was measured after 10 min in 40 μM ^{59}Fe-labeled $FeCl_3$ in three independent experiments. Compared with the empty vector control, expression of all three proteins significantly increased the iron content in yeast cells (fold increase; P value). Significant differences among the transformants are indicated by different letters as determined by analysis of variance followed by the Student-Newman-Keuls (SNK) test (P < 0.05; see Methods for details).

prokaryotic transporters of this family are composed of independent permease and ABC protein subunits (Higgins, 2001). Here, the permease subunits represent the integral membrane proteins and form the pore, whereas the soluble ABC subunits bind to the permeases and energize the transport by ATP cleavage. Several soluble, potential ABC subunits, which are predicted to be located in plastids, exist in plants and might represent interacting partners of PIC1 (Garcia et al., 2004). Among them, the gene *GCN1*, which encodes two soluble ABC subunits, is upregulated in *pic1-1* knockout mutants (Table 1). Thus, a function of PIC1 in membrane transport processes most likely has been evolutionarily conserved.

pic1 Mutant Plants Display a Severe Chlorotic Phenotype

PIC1 is expressed ubiquitously throughout all organs and developmental stages of *Arabidopsis* (Figure 3). In agreement with an essential function in chloroplasts, *PIC1* transcript abundance peaked in green tissues. However, *PIC1* is also expressed in roots and therefore might fulfill a similar function at the inner envelope of root plastids as well.

Two independently derived T-DNA insertion lines of *PIC1* (*pic1-1* and *pic1-2*) could be characterized as knockout mutations. Both mutant alleles generated the same phenotype in the homozygous progeny (Figure 5). Furthermore, we were able to complement the phenotype of *pic1-1* by the gene *PIC1* under the control of its own promoter. Thus, it is evident that the loss of PIC1 was responsible for the described phenotype. Interestingly, ~10% residual transcript fragments of *PIC1* were detected in *pic1-1/pic1-1* and *pic1-2/pic1-2* (Figure 4C). However, these transcripts lacked the N-terminal part of the PIC1 coding sequence; therefore, they could not function as templates for the synthesis of functional PIC1 proteins. Most likely, these transcript fragments originated from an ectopic promoter activity of the T-DNA insert.

pic1 knockout mutants developed severe chlorosis and only grew heterotrophically. Hence, PIC1 function is necessary for chlorophyll synthesis and/or accumulation and is a prerequisite for proper photosynthesis as well as carbohydrate assimilation in chloroplasts. Differential regulation of transcript and protein levels of genes related to photosynthesis in *pic1* mutants (see below) emphasizes this observation. As demonstrated by transmission electron microscopy, functional thylakoid membrane systems did not develop in the homozygous *pic1-1* mutant. Because rudimentary thylakoid membranes were present in plastids of cotyledons and the meristem of *pic1-1/pic1-1* but not in mature rosette leaves, we conclude that thylakoid biogenesis in *pic1-1/pic1-1* is arrested at a proplastid-like stage. This is consistent with the observation that young leaf organs of *pic1* mutants were pale green and contained some chlorophyll but turned chlorotic while growing. As a consequence, vesicle formation inside plastids of rosette leaves suggests that inchoate thylakoids are degraded during maturation of the leaf (Figures 7E and 7F). Furthermore, the fact that mutant leaves contain smaller and fewer plastids than wild-type leaves suggested a parallel organelle decomposition as well (Figure 6H). However, residual but fewer plastids without thylakoids remained in leaf cells, probably necessary for biosynthetic functions apart from pho-

tosynthesis (for functions of plastids, see Möller, 2005). This phenotype of *pic1* mutants was emphasized by the presence of transcripts and proteins associated with housekeeping functions of the chloroplast (see below).

A Role of PIC1 in Iron Transport across the Chloroplast Inner Envelope

Growth complementation on low iron supply of a yeast mutant defective in iron uptake, and uptake assays using radiolabeled Fe, showed that PIC1 and its homolog sll1656 from *Synechocystis* are capable of mediating membrane transport of iron. Thus, to our knowledge, PIC1 appears to be the first protein shown to be involved in iron transport across plastid membranes. Other chloroplast proteins with a role in metal ion transport across the chloroplast envelope are the copper-transporting ATPases PAA1 and HMA1 and the magnesium transport protein MRS2-11 (Shikanai et al., 2003; Abdel-Ghany et al., 2005; Drummond et al., 2006; Seigneurin-Berny et al., 2006). As most of the plant transporters involved in metal ion transport across the plasma membrane or the tonoplast, such as ZIP or NRAMP proteins, usually transport a broad range of heavy metal ions (Colangelo and Guerinot, 2006), it cannot be excluded that PIC1 and sll1656 might transport other metal ions besides iron as well. Because PIC1 and sll1656 were able to complement the Cu uptake–deficient yeast mutant *ctr1*, a function in copper transport might be possible. However, because of the Cu dependence of Fe uptake in yeast (Dancis et al., 1994b), it is not yet clear whether the observed complementation of *ctr1* is a result of restored copper or iron transport. Moreover, we think that the phenotypes, differential gene expression, and metal content in the *pic1* mutants favor a function in iron rather than copper transport (see discussion below).

In short-term uptake studies with radiolabeled Fe, PIC1 and sll1656 showed iron uptake rates that were much lower than those mediated by IRT1 (Table 2). These lower Fe uptake rates were in agreement with a retarded and weaker growth complementation of yeast cells on iron-limiting medium by PIC1 and sll1656 (Figure 9). A similar difference from IRT1-mediated Fe uptake in yeast has been observed in yeast cells expressing metal transporters of the NRAMP family (Curie et al., 2000; Thomine et al., 2000; Kaiser et al., 2003). Furthermore, because our assay relied on the expression of a plastid protein in yeast, it is most likely that iron uptake was mediated by a certain amount of plasma membrane–localized, mistargeted protein, explaining the low Fe uptake rates compared with the plasma membrane–intrinsic IRT1.

Chlorosis, caused by the inhibition of chlorophyll synthesis and chloroplast development (Briat and Lobreaux, 1997), is a classical symptom of iron deficiency in leaves and particularly in plastids. Furthermore, in iron-deficient leaves, the palisade parenchyma cells do not differentiate properly, and in chloroplasts, grana stacks of thylakoids are reduced drastically (Henriques et al., 2002; Varotto et al., 2002). In the case of *pic1* knockout plants, we propose that the transport pathway of iron is blocked at the inner chloroplast envelope, causing the described iron deficiency symptoms: chlorosis, lack of cell differentiation in leaf mesophyll parenchyma, and impaired thylakoid development.

Because *pic1* knockout mutants were able to germinate and develop rudimentary thylakoids in plastids of cotyledons and pale green young rosette leaves, an alternative iron uptake pathway seems to exist in *Arabidopsis* plastids. Possible by-passing transporters could be plastid-localized, iron-transporting proteins, such as NRAMP1 (Curie et al., 2000) and NRAMP6, which contain potential chloroplast transit peptides (for review, see Curie and Briat, 2003; Colangelo and Guerinot, 2006). Interestingly, both of these genes were slightly upregulated in *pic1-1* mutants (Table 1). NRAMP1 has a function in *Arabidopsis* roots (Curie et al., 2000), but according to the data of the AtGenExpress consortium (Schmid et al., 2005), transcripts of NRAMP1 are further present in the vegetative shoot apex and flowers, whereas NRAMP6 is very specifically expressed at later stages in seed development. Thus, it might be possible that these metal transport proteins confer a weak iron supplementation to *pic1* mutant plastids in seeds and meristematic tissues.

The described phenotype of *pic1* mutants as well as the in vitro iron uptake mediated by PIC1 both suggest an in vivo function in iron import into the plastid. However, impaired metal homeostasis and ferritin accumulation in *pic1* mutants might also be caused by disturbed copper transport, a defect in iron export from the plastid, or inefficient iron mobilization for Fe-S cluster assembly in chloroplasts (see below). With regard to the strong sink activity for Fe exerted by the plastidic expression of ferritin (Van Wuytswinkel et al., 1998), a role of PIC1 in iron export becomes unlikely. In conclusion, PIC1 most likely functions in Fe uptake into chloroplasts, but other roles in plastid metal ion homeostasis and transport (e.g., Fe export, Cu import/export) might be possible.

Loss of PIC1 Disturbs Metal Homeostasis in Leaves

In addition to structural changes in *pic1* knockout lines that resemble iron deficiency, leaf cells apparently experience iron stress and perturbed metal homeostasis. Unfortunately, we were not able to isolate intact plastids from *pic1* knockout plants to determine their iron content. However, when we measured the iron content in a total leaf extract from homozygous *pic1-1* plants, it was not altered relative to that of wild-type leaves. Furthermore, we were not able to rescue the *pic1* mutant phenotype by the addition of exogenously supplied Fe chelates {Fe(III)-EDTA, Sequestren [Fe(III)-EDDHA]}. When we tested the knockout mutants *pic1-1* and *pic1-2* grown on agar plates (1% sucrose, $0.5\times$ MS salts) under iron-deficient (addition of 300 μM ferrozine), iron-sufficient, and iron-abundant [addition of 50 μM Fe(III)-EDTA] conditions, we did not detect significant differences in the mutant phenotype. Furthermore, homozygous *pic1-3* mutants in this assay did not display a phenotype compared with wild-type plants. In all plants analyzed for plus/minus iron, we monitored *PIC1* transcripts by quantitative RT-PCR, which demonstrated no regulation of *PIC1* expression by iron (data not shown). In publicly available microarray data, *PIC1* was constitutively expressed under all biotic and abiotic impacts described (e.g., light, hormones, stress, Pb and Zn tolerance, and phosphate and potassium deficiency). Moreover, expression of the permease was under the control of neither iron nor zinc (Talke et al., 2006; M.L. Guerinot, E. Rogers, and U. Krämer, personal

communication). Thus, these results show that *PIC1* represents a constitutive and essential gene in *Arabidopsis* that seems not to be regulated by exogenous metal availability, like the iron uptake transporter IRT1 in roots (Eide et al., 1996; Connolly et al., 2002; Vert et al., 2003).

But what happens to metal homeostasis of the plant cell when PIC1 function is lost? In *pic1* mutant plants, ferritin proteins accumulated in plastids to much higher levels than in wild-type plants. A major role of ferritin is to precipitate Fe in the inner core of the ferritin protein cluster and thus to withdraw iron from an intracellular generation of reactive oxygen species (for overview, see Briat et al., 1999; Connolly and Guerinot, 2002). The unusual accumulation of ferritin in *pic1* knockout mutants was documented by electron microscopy (Figures 7H and 7I) at the transcript level (Table 1) as well as at the protein level (Figure 8). Thus, the increase in ferritin protein and the formation of ferritin clusters in mutant plastids was accompanied by the upregulation of *FER1* and *FER4*. Iron overload in plants has been described to cause severe oxidative stress, because free and excess Fe^{2+} ions lead to the formation of hydroxyl radicals via the Fenton reaction (Briat and Lobreaux, 1997). As a consequence, plants upregulate Cu-dependent as well as Fe-dependent superoxide dismutases (CSD and FSD) (Kliebenstein et al., 1998; Asada, 1999, Abdel-Ghany et al., 2005). Interestingly, the Cu content of *pic1-1* shoots was twice as great as in wild-type shoots, whereas the Fe levels were the same (see Supplemental Table 1 online). Compared with the wild type, *CSD1* (cytosolic) and *CSD2* (plastid-localized) increased parallel to the Cu content in leaves of *pic1* mutants, whereas transcripts and protein levels of the major plastid-localized iron superoxide dismutase (*FSD1*) were slightly downregulated, suggesting a shortage of usable iron in plastids. Furthermore, most transcripts that were increased in homozygous *pic1-1* are supposed to function in stress-related processes (data not shown), suggesting that *pic1* knockout mutants suffer from cytosolic iron stress, plastidic iron shortage, and a general copper overload. In conclusion, we propose that PIC1 function is closely linked to metal homeostasis in plastids and the cytosol.

To understand the integration of PIC1 into the metal homeostasis of the cell, we screened for differentially expressed metal transport proteins in *pic1-1* mutants (Table 1). Besides *NRAMP1* and *NRAMP6* (see above), we found the putative Fe-nicotianamine transporter *YSL1* to be upregulated in *pic1-1*. YSL1 has been shown to be involved in the loading of iron into seeds, and the expression of YSL1 is increased in response to iron excess (Le Jean et al., 2005; Waters et al., 2006). Although YSL1 as its relative YSL2 in *Arabidopsis* most likely is localized in the plasma membrane, it is discussed that the protein might be involved in Fe detoxification in specific cellular compartments (Le Jean et al., 2005). By contrast, transcripts of the iron uptake transporter IRT1, which is induced by iron deficiency in roots (Eide et al., 1996; Connolly et al., 2002; Vert et al., 2003), are decreased in *pic1-1*. Because IRT1 signals were at the detection limit of the Affymetrix microarray, we verified this observation by quantitative RT-PCR (see Supplemental Figure 2 online). Interestingly, compared with wild-type signals, IRT1 transcripts in *pic1-1* and *pic1-2* were decreased under iron-sufficient and iron-abundant conditions but not under iron deficiency, indicating that *IRT1*

expression was repressed more strongly in *pic1* mutants than in the wild type. Thus, the loss of PIC1 might interfere with iron-triggered signal transduction within the cell.

Furthermore, expression of the copper-transporting ATPase PAA1 (inner envelope of chloroplasts) (Abdel-Ghany et al., 2005) and the potential high-affinity Cu uptake protein COPT2 (for overview, see Colangelo and Guerinot, 2006) was downregulated. Thus, expression of genes related to iron stress and metal transport in *pic1* mutants reflects iron deficiency in plastids (*FSD1*, *NRAMP1*, and *NRAMP6*), iron overload in the cytosol (*FER1*, *FER4*, *CSD1*, *YSL1*, and *IRT1*), and an increased copper content in leaves (*CSD2*, *PAA1*, and *COPT2*). The described phenotype of *pic1* knockout plants (ferritin increase, IRT1 decrease, and oxidative stress) and complementation of the copper uptake–deficient yeast mutant *ctr1* by PIC1 and sll1656 (see above) suggest a role of PIC1 in Cu transport across the inner chloroplast envelope. In this case, however, quantitatively more Fe but less or unchanged Cu content should be expected in shoots of *pic1* mutants relative to wild-type shoots, as has been shown for mutants of the Cu-transporting ATPases PAA1 and HMA1 in chloroplast envelopes (Abdel-Ghany et al., 2005; Seigneurin-Berny et al., 2006). In contrast with this expectation, we made the observation that Cu concentrations in *pic1* mutant shoots were increased twofold and Fe levels did not change. Moreover, genes that have been reported to be upregulated under Cu but not under Fe deficiency (e.g., *COPT2* [Wintz et al., 2003]) apparently were not upregulated in *pic1*. In summary, we conclude that the block of iron transport in plastids of *pic1* knockout mutants causes impaired metal homeostasis, resulting in the described phenotype and regulation of gene expression.

In addition to induction by an excess of iron, ferritin accumulation in leaf chloroplasts can be induced by reactive oxygen species (specific for the isoform *FER1*) or during senescence as a result of the decomposition of the photosynthetic apparatus and the release of iron from degraded Fe-S cluster proteins (Briat et al., 1999). In contrast with the long-term storage of iron in seeds, the leaf ferritin functions as a transient iron buffer for important iron-dependent processes such as photosynthesis and nitrogen fixation. In *pic1* mutants, however, iron mobilization from ferritin seems to be defective for Fe-S cluster assembly in chloroplasts (see below), leading to the described Fe-deficiency symptoms of *pic1* mutant plastids and a simultaneous accumulation of ferritin clusters.

Plastids of *pic1* Mutants Lose Their Photosynthetic Capacity and Downregulate the Fe-S Cluster Biogenesis Machinery but Maintain Housekeeping Functions

In contrast with stress-related genes, all genes associated with photosynthesis and carbon assimilation were massively downregulated in *pic1* mutants (Table 1, Figure 8). This decrease in photosynthesis-associated proteins is reflected by the phenotype of *pic1* mutants, characterized by heterotrophic growth, chlorosis, and the degradation of thylakoids in plastids. Fe-S cluster proteins are central for the function of the photosynthetic electron transport chain in chloroplasts (Raven et al., 1999). The assembly of these Fe-S proteins takes place in plastids and involves the action of desulfurases and scaffold proteins, which synthesize transient Fe-S clusters (for overview, see Balk and Lobreaux, 2005; Ye et al., 2006). Whereas elemental sulfur is provided by the desulfurases, iron is mobilized via a yet unknown pathway and transferred to the scaffold proteins. To understand the possible implication of PIC1 in Fe-S cluster biogenesis, we monitored the transcript abundance of all genes described either to function in the Fe-S biogenesis machinery or to code for the major, plastid-localized Fe-S cluster–containing proteins (Ye et al., 2006) in homozygous *pic1-1* mutants by microarray analysis (Table 3). Differential gene expression in *pic1-1* versus the wild type was further analyzed by SAM software (Tusher et al., 2001). Interestingly, gene expression of the desulfurase Cp *NifS* and the desulfurase activator Cp *SufE* was not differentially regulated, whereas the scaffold proteins Nfu1, Nfu2, Nfu3, and Cp IscA, which are proposed to integrate iron into the *Arabidopsis* chloroplast Fe-S clusters (Ye et al., 2006), were downregulated in *pic1-1* mutants. By contrast, expression of the corresponding mitochondrial proteins ISU1 (desulfurase), Nfu4, and Nfu5 (scaffold) was not changed or increased, respectively. Thus, PIC1 function might be involved in the mechanism of iron mobilization for Fe-S cluster assembly in chloroplasts.

Furthermore, expression of several chloroplast-localized Fe-S cluster proteins in *pic1-1* was downregulated (Table 3). These include the major leaf ferredoxins (FED A and FD1) and ferredoxin–thioredoxin reductases (FTR β and FTR-A), the chlorophyllide *a* oxygenase CAO (for chlorophyll *b* biosynthesis), and enzymes for sulfur assimilation (the adenosine-5-phosphate reductases APR1 to APR3 and the sulfite reductase SiR). Again, transcripts of mitochondrial ferredoxins (the adrenodoxin-like ferredoxins adr.-l Fd1 and adr.-l Fd2) were not changed or increased. Expression of Fe-S proteins for chlorophyll breakdown (PaO, for pheophorbide *a* oxygenase) and siroheme biosynthesis (SirB, for sirohydrochlorin ferrochelatase), however, was not changed. Interestingly, siroheme in plants is found as a prosthetic group only for the plastid-localized sulfite and nitrite reductases, and the iron required for siroheme biosynthesis by SirB is probably acquired via a pathway distinct from that for Fe-S cluster assembly (Raux-Deery et al., 2005).

Transcripts of genes coding for Fe-S proteins with housekeeping functions in plastids such as protein import (*Tic55*, a member of the translocon at the inner envelope of chloroplasts) as well as the chloroplast-localized nitrogen fixation machinery (*NIR*, for nitrite reductase; *GLU1* and *GLU2*, two ferredoxin-dependent GOGATs [glutamine:2-oxo-glutarate amido transferases]; *GLT1*, an NADH-dependent GOGAT; and *Atase 2*, for amidophosphoribosyltransferase) were unchanged in *pic1-1* (Table 3) (Ye et al., 2006), indicating that *pic1* mutant chloroplasts are able to import precursor proteins (see below) and to assimilate nitrogen. Other genes, encoding non–Fe-S proteins with housekeeping functions in the chloroplast stroma or envelope (e.g., the major protein import pore Toc75 and the amino acid–selective channel OEP16), also are not regulated in *pic1* mutants (Table 1, Figure 8). Thus, although *pic1* mutant plastids are deranged in metal homeostasis, lose their photosynthetic capacity, and most likely are impaired in Fe-S cluster biogenesis, they seem to provide housekeeping functions. This is underlined by the fact that *pic1* mutant plants are able to survive when

Table 3. Expression of Genes Related to Fe-S Cluster Biogenesis and Fe-S Proteins in Chloroplasts and Mitochondria of Homozygous *pic1-1* and Wild-Type Plants

Gene	AGI Code	Signal, *pic1-1*	Signal, Wild Type	Change Direction	Fold Change	P Value	Subcellular Localization
Fe-S biogenesis							
CpNifS	At1g08490	69 ± 4.8	120 ± 44	No			C
CpSufE	At4g26500	98 ± 11	88 ± 12	No			C
Nfu1	At4g01940	297 ± 26	430 ± 104	No			C
Nfu2	At5g49940	401 ± 19	709 ± 58	Down	0.57	0.01693783	C
Nfu3	At4g25910	237 ± 37	347 ± 33	Down	0.68	0.053113348	C
CpIscA	At1g10500	265 ± 22	479 ± 20	Down	0.55	0.007358573	C
ISU1	At4g22220	562 ± 32	610 ± 98	No			M
Nfu4	At3g20970	153 ± 5.0	110 ± 9.0	Up	1.39	0.018084881	M
Nfu5	At1g51390	49 ± 6.1	32 ± 7.7	Up	1.54	0.053113348	M
Fe-S proteins							
FED A	At1g60950	2594 ± 187	4552 ± 379	Down	0.57	0.019719323	C
FD1	At1g10960	1628 ± 285	2930 ± 371	Down	0.56	0.032460585	C
adr.-l Fd1	At4g21090	125 ± 18	67 ± 7.5	Up	1.87	0.027014065	M
adr.-l Fd2	At4g05450	70 ± 8.6	83 ± 14	No			M
FTR β	At2g04700	528 ± 81	1179 ± 131	Down	0.45	0.019719323	C
FTR-A	At5g08410	174 ± 24	337 ± 55	Down	0.52	0.032460585	C
CAO	At1g44446	167 ± 14	477 ± 118	Down	0.35	0.038748737	C
APR1	At4g04610	73 ± 14	451 ± 113	Down	0.16	0.027014065	C
APR2	At1g62180	296 ± 35	683 ± 114	Down	0.43	0.027014065	C
APR3	At4g21990	67 ± 5	370 ± 55	Down	0.18	0.014534325	C
SIR	At5g04590	278 ± 10	411 ± 49	Down	0.67	0.038748737	C
PaO	At3g44880	100 ± 22	148 ± 32	No			C
SirB	At1g50170	185 ± 5.9	187 ± 11	No			C
Tic55	At2g24820	148 ± 8.1	225 ± 50	No			C
NIR	At2g15620	323 ± 17	413 ± 83	No			C
GLU1	At5g04140	421 ± 65	1191 ± 422	No			C
GLU2	At2g41220	79.5 ± 12	89 ± 33	No			C
GLT1	At5g53460	458 ± 92	308 ± 66	No			C
ATase2	At4g34740	100 ± 15	62 ± 23	No			C

Affymetrix ATH1 microarray analysis was performed on 14-d-old seedlings of *pic1-1* mutant and Col-0 wild-type plants as described in Methods. The average scaled signals ($n = 3$; ±SD) are shown. Signal differences were evaluated by SAM software (Tusher et al., 2001), resulting in change direction, fold change, and corresponding significance measures (P value, false discovery rate = 5.31%). For details of the analysis, see Methods and Supplemental Table 2 online. Please note that we listed all genes reported to be involved in the plastidic Fe-S cluster biogenesis machinery as well as all major plastid-localized Fe-S proteins described by Ye et al. (2006) and corresponding mitochondrial proteins. Thus, several genes listed are not differentially expressed (no change). The Arabidopsis Genome Initiative (AGI) code for each gene is given, and the subcellular localization of the corresponding protein is designated as follows: C, chloroplasts; M, mitochondria.

supplemented with sucrose and are still able to accumulate anthocyane pigments, which requires biosynthetic steps in plastids.

PIC1 and Its Possible Implication in Protein Transport

A very recent report (Teng et al., 2006) describes the protein At2g15290 (PIC1) as part of the protein translocon of the inner envelope in chloroplasts (Tic21). The knockout mutant *cia5-3* described in that article is identical to *pic1-1* described here. Furthermore, all At2g15290 knockout alleles show the same chlorotic phenotype.

Teng and coworkers (2006) detected very few residual precursor proteins of OE33 (PSBO-1) and POR by immunoblot analysis within their *cia5* mutant, suggesting a defect in chloroplast protein import. In our immunoblot analyses, however, we could not detect residual precursor proteins of PSBO-1 and POR or of any other proteins tested in *pic1* mutants (Figure 8). By

contrast, we found increased levels of mature proteins (e.g., ferritin or CSD2 in mutant plastids) (Figures 7 and 8). Further studies by Teng et al. (2006) to elucidate the function of At2g15290 in protein import into chloroplasts were performed with transgenic *Arabidopsis* ectopically expressing At2g15290 under the control of the 35S promoter. The mild mutant used in their import experiments still showed a strong phenotype (i.e., mosaic pale green leaves and reduced growth). Thus, complementation was not complete and the still severe physiological defects might implicate further and pleiotropic loss or restriction of unrelated genes and functions. In our hands, complementation only by the authentic *PIC1* promoter yielded full recovery, whereas 35S-controlled ectopic *PIC1* expression caused severe pleiotropic effects (data not shown). In conclusion, we think that impaired import of certain precursor proteins into *cia5/pic1* mutant plastids is an indirect effect resulting from defective metal homeostasis as well as retarded plastid development caused by PIC1 function in iron transport and/or mobilization. As

shown in Figure 8, several proteins are very well imported and processed within *pic1* mutant plastids.

In our opinion, the described chlorotic and dwarfed phenotype of *pic1* knockout mutants closely links PIC1 to metal homeostasis of chloroplasts. Although PIC1 shows sequence homology with prokaryotic solute permeases and not with known protein import pores with four α-helical transmembrane domains (e.g., Tim proteins in the inner membrane of mitochondria [Murcha et al., 2007]), a function of the protein in the translocation of precursor proteins cannot be fully excluded. Finally, the functional complementation of iron uptake–defective yeast mutants and the measured iron uptake, mediated by PIC1 and sll1656, clearly provide evidence for their function in iron transport and metal homeostasis.

METHODS

Plant Material and Growth Conditions

All experiments were performed on *Arabidopsis thaliana* plants, ecotype Col-0 (Lehle Seeds). The T-DNA insertion lines SALK_104852 (*pic1-1*), GABI 577D06 (*pic1-2*), and 804F07 (*pic1-3*) were purchased from NASC (University of Nottingham) and GABI-Kat (Max Planck Institute for Plant Breeding Research). Before sowing, seeds were surface-sterilized with ethanol and 5% hypochloride. To synchronize germination, all seeds were kept at 4°C for 3 d. Plants were grown on soil or on 0.3% Gelrite medium (Serva) containing 1% D-sucrose and 0.5× MS salts at pH 5.7. Plant growth occurred in growth chambers with a 16-h light (21°C; photon flux density of 100 μmol·m^{-2}·s^{-1}) and 8-h dark (16°C) cycle.

Protein Import Experiments

Intact chloroplasts for import experiments were isolated from 8-d-old *Arabidopsis* seedlings according to Aronsson and Jarvis (2002). The cDNA of At-*PIC1* was purchased as SSP pUNI51 clone U18531 (Yamada et al., 2003). For in vitro transcription, PIC1 was subcloned into pGEM 4-Z (*Eco*RI/*Sac*I) (Promega). In vitro transcription was performed using the mMessage mMachine kit (Ambion). Translation and protein import of the precursor protein PIC1 were performed as described by Nada and Soll (2004). The import reaction contained *Arabidopsis* chloroplasts equivalent to 10 μg of chlorophyll and 4.5 μL of in vitro translation product in 100 μL of import buffer.

Antiserum Production and Immunoblot Analysis

To raise an antiserum against At-PIC1, the C-terminal end of the PIC1 cDNA was amplified by PCR on PIC1/pUNI51 using the oligonucleotide primers PIC1(−154)-Ncofw (5′-TGCCATGGTTTTCTGGTCGTTTGGGTA-TATTC-3′) and PIC1fl-Xhorev (5′-GGCAGACTCGAGAGCAACCTTAG-GAACTAC-3′). The resulting truncated version PIC1(−154), which lacks the first 154 amino acids of the protein, was subcloned into the pPROEx Hta (*Nco*I/*Xho*I) plasmid vector (Invitrogen). The generated plasmid PIC1(−154)/pPROEx Hta was used for overexpression after transforming *Escherichia coli* BL21(DE3) cells (Novagen/Merck Biosciences). Rapidly growing cells with an OD$_{600}$ of 0.6 were induced with 0.6 mM isopropyl 1-thio-β-D-galactopyranoside for 3 h at 37°C. Afterward, pelleted cells were resuspended in cell lysis solution (50 mM Tris-HCl, pH 8.0, 25% [w/v] sucrose, 1 mM EDTA, and 100 μg/mL DNase) and sonicated three times for 30 s. Inclusion bodies were collected by centrifugation at 4°C and 20,000g for 30 min. The resulting pellet was resuspended in buffer A (50 mM NaPP, pH 8.0, 100 mM NaCl, 2 mM β-mercaptoethanol, and 8 M urea) and sonicated again. Remaining insoluble material was pelleted by

centrifugation (4°C, 20,000g, 30 min). The major fraction of overexpressed recombinant PIC1(−154) protein was present in the urea-soluble supernatant. Proteins in this fraction were separated by SDS-PAGE, and the overexpressed PIC1(−154) of 15 kD was recovered by electroelution. The protein was concentrated using an Amicon ultrafiltration cell with YM10 membranes (Millipore) in 25 mM Tris-HCl, pH 8.0, 0.19 M Gylcin, 5 mM β-mercaptoethanol, and 1% (w/v) SDS and used as antigene to raise antibodies in rabbit (BioGenes). Polyclonal antisera against Nt-RBCS, At-OEP16.1, Ps-VIPP1, and At-PORB were raised in rabbit (Pineda Antibody Service); anti-Lhcb4 antiserum was purchased from Agrisera.

Subfractionation of chloroplasts from 6-week-old *Arabidopsis* rosette leaves was performed as described by Gerdes et al. (2006). For a total protein extract from 4-week-old leaves, plant material was homogenized in liquid nitrogen and proteins were extracted in 50 mM Tris-HCl, pH 8, 50 mM EDTA, 2% lithium dodecyl sulfate, 10 mM DTT, and 100 μM phenylmethylsulfonyl fluoride on ice for 30 min. Cell debris was pelleted by 15 min of centrifugation (4°C, 14,000g). Proteins from envelopes, stroma, and thylakoid membranes or from leaves of *pic1* mutants and wild-type plants were separated by SDS-PAGE and subsequently transferred to nitrocellulose filters. The antisera against PIC(−154) and PORB were used in a 1:500 dilution, antiserum against At-FER was used at 1:2500, and all other antisera were diluted 1:1000; secondary anti-rabbit IgG alkaline phosphatase antibodies (Sigma-Aldrich) were diluted 1:30,000. Nonspecific signals were blocked by 1% skim milk powder and 0.3% BSA. Blots were stained using the alkaline phosphatase reaction in the presence of nitroblue tetrazolium and bromochloroindolyl phosphate as substrate; for FER detection, blots were stained with the Immobilon Western kit (Millipore) using the chemiluminescent alkaline phosphatase substrate.

Subcellular Localization of GFP Fusion Proteins

To generate a C-terminal fusion of GFP to the preprotein At-PIC1, the entire coding sequence was amplified by PCR using the primers flGATE fw (5′-CACCATGGCAATCACTACTCTTGCCGCC-3′) and flGATE rev (5′-AGCAACCTTAGGAACTACGACAG-3′) on PIC1/pUNI51. Accordingly, the cDNA of At-*OEP7* was amplified by OEP7forGFP (5′-AAAAAG-CAGGCTATATGGGAAAAACTTCGGGAG-3′) and OEP7revGFP (5′-AGA-AAGCTGGGTACAAACCCTCTTTGGATGTGG-3′) on *Arabidopsis* Col-0 cDNA. The resulting PCR products were subcloned into the binary pK7FWG2 vector (Karimi et al., 2002) using the Gateway cloning system (Invitrogen). pK7FWG2 provides a fusion of GFP to the C-terminal end of the respective proteins, which are expressed under the control of the constitutive 35S cauliflower mosaic virus promoter.

Arabidopsis mesophyll protoplasts were isolated from leaves of 4-week-old plants and transiently transfected with PIC1/pK7FWG2 and OEP7/pK7FWG2 according to the protocol of the Sheen Lab (http://genetics.mgh.harvard.edu/sheenweb/protocols_reg.html). After 16 h of expression, fluorescence images were obtained with an epifluorescence microscope (polychrome IV system; Till Photonics) using GFP and fluorescein isothiocyanate filter sets. Photographs were taken with a cooled infrared CCD camera and visualized with the TILLvision 4.0 software.

Transcript Level Profiling

To monitor transcript abundance, total RNA was extracted from the respective *Arabidopsis* tissues using the Plant RNeasy extraction kit (Qiagen). In general, three samples were harvested for each tissue type from 10 (for mature plants) to 500 (for seedlings) individual plants to decrease biological variation.

For microarray analysis, 5 μg of RNA from 14-d-old seedlings of the *pic1-1* mutant and the wild type was processed and hybridized to Affymetrix GeneChip Arabidopsis ATH1 Genome Arrays using the Affymetrix One-Cycle Labeling and Control (Target) kit according to the

manufacturer's instructions. To provide biological replicates, RNA for each sample was isolated from at least 40 individual seedlings. Furthermore, three mutant and three wild-type samples ($n = 3$) were grown and harvested with a time interval of 1 week. Microarray signals were made comparable by scaling the average overall signal intensity of all probe sets to a target signal of 100. Signals from *pic1-1* ($n = 3$) and the wild type ($n = 3$) were analyzed by Affymetrix Data Mining Tool and GeneChip Operating software (compare with Clausen et al., 2004). The statistical significance of signal differences was evaluated by SAM software (Tusher et al., 2001). Here, we performed a two-class unpaired *t* test on the signal values (number of permutations = 100). Setting the delta cutoff value at 1.55 resulted in a data set of 4235 significantly regulated genes with a false discovery rate of 5.31%.

The RNA used in quantitative real-time RT-PCR was digested with DNase and reverse-transcribed into cDNA (Clausen et al., 2004). Detection and quantification of transcripts were performed as described previously (Philippar et al., 2004) using a LightCycler (Roche). For *PIC1*, we constructed the gene-specific primers LCfw (5′-CTCCGTCGAACTT-CCA-3′) and LCrev (5′-AACTACGACAGATTCCG-3′), amplifying a product of 333 bp. To prevent the amplification of contaminating genomic DNA, the primers were selected to flank introns 2 and 3 (Figure 4A). To analyze the residual N-terminal RNA in the mutants *pic1-1* and *pic1-2*, the primer pair pic1,2 fw (5′-AGAACACCAATTCGCTAC-3′) and pic1,2 rev (5′-CCTCATTATCACCGGG-3′) was designed to amplify a product of 343 bp, spanning both sites of the T-DNA insertion. All quantifications were normalized to the signal of actin cDNA fragments generated by the primers Act fw (5′-GGTGATGGTGTGTCT-3′) and Act rev (5′-ACTGAGC-ACAATGTTAC-3′), which amplified cDNA from actin 2 and 8 (At3g18780 and At1g49240).

Data used to create in silico transcriptional profiles were obtained from the AtGenExpress developmental series leaves, shoots and stems, and roots at the NASCArrays website (http://affymetrix.Arabidopsis.info/narrays/experimentbrowse.pl.).

Characterization of the T-DNA Mutants *pic1-1*, *pic1-2*, and *pic1-3*

Genomic DNA of the heterozygous T-DNA insertion lines inside At-*PIC1*, *pic1-1* (SALK_104852) (Alonso et al., 2003), *pic1-2* (GABI-Kat 577D06), and *pic1-3* (GABI-Kat 804F07) (Rosso et al., 2003) was screened by PCR genotyping. *PIC1* gene-specific primers in combination with T-DNA–specific left border primers generated fragments of 524 bp (*pic1-1*), 716 bp (*pic1-2*), and 738 bp (*pic1-3*) on heterozygous and homozygous plants. To identify plants with the T-DNA insertion in both alleles of *PIC1*, we used gene-specific primers flanking the predicted T-DNA insertion sites. DNA from homozygous, mutated *pic1* gave no amplification product, whereas the amplified regions on wild-type and heterozygous DNA were 434 bp (*pic1-1*), 582 bp (*pic1-2*), and 519 bp (*pic1-3*). The following primers were used: for *pic1-1*, 52fw (5′-GTTTCGTTGTCCGCTGGC-TTTAGC-3′) and 52rev (5′-GGTTAAATGAGTGCTGGAAACCTGGC-3′); for *pic1-2*, 77fw (5′-TGCAATCACTACTCTTGCCGCCGG-3′) and 77rev (5′-CAATCTCTTTGCAACCTGTGAATA-3′); for *pic1-3*, 04fw (5′-GTTCC-TGTCTCAGTTCTTTATGCC-3′) and 04rev (5′-CAACAACTACCTCCTAT-CACGATG-3′); as well as SALK LBb1 (5′-GCGTGGACCGCTTGCTG-CAACT-3′) and GABI LB1 (5′-CCCATTTGGACGTGAATGTAGACAC-3′). For positions and orientations of the T-DNA inserts and oligonucleotide primers, see Figure 4A. To verify PCR products and T-DNA insertion sites, all amplified DNA fragments were sequenced.

To complement the mutant *pic1-1*, a 3327-bp genomic fragment of *PIC1* (g*PIC1*) was amplified by PCR on genomic DNA of Col-0 wild-type plants and subcloned into the binary plasmid vector pKWG (Karimi et al., 2002) using the Gateway cloning system (Invitrogen). The primers used to clone g*PIC1* were gPIC1fw (5′-GTCAAACCTGAGTCTGATTTCTCTTC-3′) and gPIC1rev (5′-AGCAACCTTAGGAACTACGACAG-3′), flanking a 1830-bp promoter region and the entire genomic sequence of *PIC1* (1497 bp). The

construct gPIC1/pKWG was transformed into chemically competent *Agrobacterium tumefaciens* GV3101 cells. Heterozygous *PIC1/pic1-1* plants (T4 generation) were transformed by vacuum infiltration as described by Bechtold et al. (1993). Transformed T1 plants were selected on kanamycin (100 μg/mL) containing agar medium (0.3% Gelrite, 1% D-sucrose, and 0.5× MS salts) and afterward transferred to soil. Plants in the T1 and T2 generations in addition were characterized by PCR genotyping. Oligonucleotide primers for the gPIC1/pKWG T-DNA were PIC1 E3fw (5′-GTTG-TGAAAGGTTTGAGGAGCG-3′) and attB2 adapter (5′-ACCACTTTGTAC-AAGAAAGCTGGGT-3′), the latter being specific for the pKWG vector. The T-DNA insertion in *pic1-1* was detected as described above, and homozygous *pic1-1/pic1-1* alleles were identified by the absence of PCR products from primers flanking the *PIC1* gene: PIC1 5′UTRfw (5′-GCC-CATTGCAACTGTGAAGAATAGACG-3′) and PIC1 3′UTRrev (5′-CATTG-AATCCGCAATCGTTGGTTCTC-3′).

Electron Microscopy

Pieces of leaf tissue were fixed immediately with 2.5% glutaraldehyde in 75 mM sodium cacodylate and 2 mM $MgCl_2$, pH 7.0, for 1 h at room temperature, rinsed several times in fixative buffer, and post-fixed for 2 h with 1% osmium tetroxide in fixative buffer at room temperature. After two washing steps in distilled water, the cells were stained en bloc with 1% uranyl acetate in 20% acetone for 30 min. Dehydration was performed with a graded acetone series. Samples were then infiltrated and embedded in Spurr's low-viscosity resin (Spurr, 1969). After polymerization, ultrathin sections with thickness between 50 and 70 nm were cut with a diamond knife and mounted on uncoated copper grids. The sections were poststained with aqueous lead citrate (100 mM, pH 13.0). All micrographs were taken with an EM 912 electron microscope (Zeiss) equipped with an integrated Omega energy filter operated in the zero loss mode. Semithin sections were cut with a diamond knife with a thickness of 500 nm and mounted on glass slides; phase contrast micrographs were taken with a Zeiss Axiophot microscope and a Nikon D1000 digital camera.

Complementation and Iron Accumulation in Yeast Mutants

For functional expression in yeast, the entire coding sequence of At-*PIC1* was amplified by PCR on the cDNA PIC1/pUNI51 using the primers flGATE fw and flGATE rev (see above). The coding sequence of *sll1656* from *Synechocystis* sp strain PCC 6803 was amplified by PCR on genomic DNA with the following primers: sllfw (5′-CACCATGAACC-GACGCAACACCG-3′) and sllrev (5′-CTTGTTCAGACGGTCTAGCAAC-CACAG-3′). After subcloning into pCR2.1 TA vector (Invitrogen), both cDNAs were subcloned into the yeast expression vectors pFL61 (*Pst*I/*Spe*I) and pDR195 (*Xho*I/*Bam*HI). The cDNA of IRT1 from *Arabidopsis* was purchased as GSLT cDNA (Castelli et al., 2004). The coding sequence of *IRT1* was amplified by PCR using the primers IRT1.NotIfw (5′-ATT-CAGGCGGCCGCATGAAAACAATCTTCCTCGTAC-3′) and IRT1.NotIrev (5′-ATCTGGGCGGCCGCTTAAGCCCATTTGGCGATAATC-3′) and subcloned into pFL61 and pDR195 digested with *Not*I.

The yeast strains used in this study were *fet3 fet4* DEY1453 (*MATα/MATα ade2/+ can1/can1 his3/his3 leu2/leu2 trp1/trp1 ura3/ura3 fet3-2::HIS3/fet3-2::HIS3 fet4-1::LEU2/fet4-1::LEU2*) (Eide et al., 1996) and *ctr1*: 64p (*MATα gcn4 his3 leu2 trp1 ura3 ctr1::LEU2*) (Dancis et al., 1994a). Untransformed mutant yeast cells were grown in YPD (yeast extract, peptone, and D-glucose) medium and, after transformation in selective synthetic complete (SC) (−uracil) minimal medium, supplemented with 20 g/L glucose and necessary auxotrophic supplements (Eide et al., 1996). For optimal growth of the *fet3 fet4* strain, the pH of YPD and SC (−uracil) was decreased to 4.0 and 3.5, respectively. Yeast cells were transformed with the respective plasmids using standard procedures (Gietz and Schiestl, 1991). For complementation experiments, 10-μL drops of yeast cultures were spotted in different dilutions onto SC

(−uracil) plates, pH 5.0, supplemented with different concentrations of FeCl$_3$ or EDTA. For iron accumulation, the *fet3 fet4* mutant transformants were grown to exponential phase in synthetic defined medium containing 30 g/L glucose, 1.7 g/L yeast nitrogen base without amino acids, 5 g/L (NH$_4$)$_2$SO$_4$, and necessary auxotrophic amino acids without uracil. This medium was also supplemented with 50 μM Fe(III)-EDTA. Cells were centrifuged for 10 min at 3500 rpm at 4°C and washed once in ice-cold ultrapure water and once in ice-cold MGN medium (10 mM MES, 3% glucose, and 1 mM nitrilotriacetic acid, pH 6.1). Cells were resuspended in MGN medium to reach an OD$_{600}$ of 4.0. Iron accumulation was assayed in MGN medium supplemented with 1 mM ascorbate and 40 μM ^{59}Fe-labeled FeCl$_3$. Cells were incubated for 15 min at 30°C before the addition of MGN medium with ^{59}Fe-labeled FeCl$_3$ (specific activity of 740 MBq/mol; Perkin-Elmer) for 10 min. Finally, cells were vacuum-filtered through Whatman GF/C filters and washed with 20 mL of ice-cold SSW solution (Eide et al., 1992). The filters were used for the determination of total activity by scintillation counting (Wallac). Mean values for iron accumulation resulted from the measurement of three replicates for each transformant. Data were subjected to one-way analysis of variance followed by a Student-Newman-Keuls test (P < 0.05) using the statistical software Sigmastat for Windows (version 2.0; Systat Software).

Computational Analysis of Protein and DNA Sequences

To identify proteins homologous with At-PIC1, BLAST searches against GenBank (http://www.ncbi.nlm.nih.gov/BLAST/; Altschul et al., 1997), PHYSCObase (http://moss.nibb.ac.jp/; Nishiyama et al., 2003), and the genome databases of *Chlamydomonas reinhardtii* (*Chlamydomonas reinhardtii* version 3.0 database; http://genome.jgi-psf.org/Chlre3/Chlre3.home.html) and *Cyanidioschyzon merolae* (*Cyanidioschyzon merolae* Genome Project; http://merolae.biol.s.u-tokyo.ac.jp/; Matsuzaki et al., 2004) were performed. COGs (Tatusov et al., 2003) are accessible at http://www.ncbi.nlm.nih.gov/COG/. The plant membrane protein database ARAMEMNON (version 3.2; http://aramemnon.botanik.uni-koeln.de/; Schwacke et al., 2003) was used to determine consensus transmembrane topologies. The phylogenetic tree was constructed with the program PAUP version 4.0b10 (Swofford, 2002). A minimal evolution tree was calculated using the default settings. In the analysis, 148 amino acids were included that were situated within or adjacent to the predicted transmembrane helices (see Supplemental Figure 1 online). The data were bootstrap-resampled 100 times. Protein sequence alignments were generated by ClustalX (Thompson et al., 1997) using the Gonnet series protein weight matrix with default settings. Promoter prediction was performed with Neural Network Promoter Prediction (http://www.fruitfly.org/seq_tools/promoter.html; Reese, 2001), and the plant TATA box was defined by MatInspector at GenomatixSuite 3.4.1 (http://www.genomatix.de; Cartharius et al., 2005).

Accession Numbers

Sequence data from this article can be found in the GenBank, GenPept, and PHYSCObase data libraries, the genome databases of *C. reinhardtii* and *C. merolae*, or under the respective *Arabidopsis* gene index (Arabidopsis Genome Initiative locus identifier): *Arabidopsis thaliana* At-PIC1 (AY057510, At2g15290); rice (*Oryza sativa*) Os-PIC1 (XM_464386, Os02g0187600) and Os-PIC2 (AP003573, Os06g0638100); maize (*Zea mays*) Zm-PIC1 (BT017876) and Zm-PIC2 (BT018285); *Lotus japonicus* Lj-PIC1 (AP006404); *Physcomitrella patens* Pp-PIC1 (contig 5795); *C. reinhardtii* PIC1 (protein identifier 178114); *C. merolae* PIC1 (protein identifier CMN128C); *Synechocystis* (sll1656, BAA16830); *Anabena* sp PCC 7120 (all4113, BAB75812); *Thermosynechococcus elongatus* BP-1 (tll0396, BAC07948); *Prochlorococcus marinus* strain MIT 9313 (PMT0365, NP_894198); and *Arabidopsis* IRT1 (BX827853, At4g19690) and OEP7 (NM_115102, At3g52420).

Supplemental Data

The following materials are available in the online version of this article.

Supplemental Figure 1. Multiple Sequence Alignment of the PIC1 Family in Eukaryotes and Cyanobacteria.

Supplemental Figure 2. IRT1 mRNA in *pic1* Mutant and Col-0 Wild-Type Plants under Iron-Sufficient, Iron-Deficient, and Iron-Abundant Conditions.

Supplemental Table 1. Fe and Cu Content in Shoots of *pic1-1* Mutant and Col-0 Wild-Type Plants.

Supplemental Table 2. Raw Array Data (Affymetrix ATH1 GeneChip) of *pic1-1* Mutant versus Wild-Type Analysis.

REFERENCES

Abdel-Ghany, S.E., Muller-Moule, P., Niyogi, K.K., Pilon, M., and Shikanai, T. (2005). Two P-type ATPases are required for copper delivery in *Arabidopsis thaliana* chloroplasts. Plant Cell **17:** 1233–1251.

Alonso, J.M., Stepanova, A.N., Leisse, T.J., Kim, C.J., Chen, H., Shinn, P., Stevenson, D.K., Zimmerman, J., Barajas, P., Cheuk, R., and Heller, C. (2003). Genome-wide insertional mutagenesis of *Arabidopsis thaliana*. Science **301:** 653–657.

Altschul, S.F., Madden, T.L., Schaffer, A.A., Zhang, J., Zhang, Z., Miller, W., and Lipman, D.J. (1997). Gapped BLAST and PSI-BLAST: A new generation of protein database search programs. Nucleic Acids Res. **25:** 3389–3402.

Aronsson, H., and Jarvis, P. (2002). A simple method for isolating import-competent Arabidopsis chloroplasts. FEBS Lett. **529:** 215–220.

Asada, K. (1999). The water-water cycle in chloroplasts: Scavenging of active oxygen and dissipation of excess photons. Annu. Rev. Plant Physiol. Plant Mol. Biol. **50:** 601–639.

Aseeva, E., Ossenbühl, F., Eichacker, L.A., Wanner, G., Soll, J., and Vothknecht, U.C. (2004). Complex formation of Vipp1 depends on its alpha-helical PspA-like domain. J. Biol. Chem. **279:** 35535–35541.

Balk, J., and Lobreaux, S. (2005). Biogenesis of iron-sulfur proteins in plants. Trends Plant Sci. **10:** 324–331.

Bechtold, N., Ellis, J., and Pelletier, G. (1993). *In planta Agrobacterium*-mediated gene transfer by infiltration of adult *Arabidopsis thaliana* plants. C. R. Acad. Sci. Paris/Life Sci. **316:** 1194–1199.

Briat, J.F., and Lobreaux, S. (1997). Iron transport and storage in plants. Trends Plant Sci. **2:** 187–193.

Briat, J.F., Lobreaux, S., Grignon, N., and Vansuyt, G. (1999). Regulation of plant ferritin synthesis: How and why. Cell. Mol. Life Sci. **56:** 155–166.

Cartharius, K., Frech, K., Grote, K., Klocke, B., Haltmeier, M., Klingenhoff, A., Frisch, M., Bayerlein, M., and Werner, T. (2005). MatInspector and beyond: Promoter analysis based on transcription factor binding sites. Bioinformatics **13:** 2933–2942 .

Castelli, V., et al. (2004). Whole genome sequence comparisons and ''full-length'' cDNA sequences: A combined approach to evaluate and improve *Arabidopsis* genome annotation. Genome Res. **14:** 406–413.

Clausen, C., Ilkavets, I., Thomson, R., Philippar, K., Vojta, A., Möhlmann, T., Neuhaus, E., Fulgosi, H., and Soll, J. (2004). Intracellular localization of VDAC proteins in plants. Planta **220:** 30–37.

Colangelo, E.P., and Guerinot, M.L. (2006). Put the metal to the petal: Metal uptake and transport throughout plants. Curr. Opin. Plant Biol. **9:** 322–330.

Connolly, E.L., Fett, J.P., and Guerinot, M.L. (2002). Expression of the IRT1 metal transporter is controlled by metals at the levels of transcript and protein accumulation. Plant Cell **14:** 1347–1357.

Connolly, E.L., and Guerinot, M. (2002). Iron stress in plants. Genome Biol. **3:** REVIEWS1024.1–REVIEWS1024.4.

Curie, C., Alonso, J.M., Le Jean, M., Ecker, J.R., and Briat, J.F. (2000). Involvement of NRAMP1 from *Arabidopsis thaliana* in iron transport. Biochem. J. **347:** 749–755.

Curie, C., and Briat, J.F. (2003). Iron transport and signaling in plants. Annu. Rev. Plant Biol. **54:** 183–206.

Dancis, A., Haile, D., Yuan, D.S., and Klausner, R.D. (1994a). The *Saccharomyces cerevisiae* copper transport protein (Ctr1p). Biochemical characterization, regulation by copper, and physiologic role in copper uptake. J. Biol. Chem. **269:** 25660–25667.

Dancis, A., Yuan, D.S., Haile, D., Askwith, C., Eide, D., Moehle, C., Kaplan, J., and Klausner, R.D. (1994b). Molecular characterization of a copper transport protein in *S. cerevisiae*: An unexpected role for copper in iron transport. Cell **76:** 393–402.

Dix, D.R., Bridgham, J.T., Broderius, M.A., Byersdorfer, C.A., and Eide, D.J. (1994). The FET4 gene encodes the low affinity Fe(II) transport protein of *Saccharomyces cerevisiae*. J. Biol. Chem. **269:** 26092–26099.

Drummond, R.S.M., Tutone, A., Li, Y.C., and Gardner, R.C. (2006). A putative magnesium transporter AtMRS2-11 is localized to the plant chloroplast envelope membrane system. Plant Sci. **170:** 78–89.

Eide, D., Broderius, M., Fett, J., and Guerinot, M.L. (1996). A novel iron-regulated metal transporter from plants identified by functional expression in yeast. Proc. Natl. Acad. Sci. USA **93:** 5624–5628.

Eide, D., Davis-Kaplan, S., Jordan, I., Sipe, D., and Kaplan, J. (1992). Regulation of iron uptake in *Saccharomyces cerevisiae*. The ferrireductase and Fe(II) transporter are regulated independently. J. Biol. Chem. **267:** 20774–20781.

Emanuelsson, O., Nielsen, H., and von Heijne, G. (1999). ChloroP, a neural network-based method for predicting chloroplast transit peptides and their cleavage sites. Protein Sci. **8:** 978–984.

Froehlich, J.E., Wilkerson, C.G., Ray, W.K., McAndrew, R.S., Osteryoung, K.W., Gage, D.A., and Phinney, B.S. (2003). Proteomic study of the *Arabidopsis thaliana* chloroplastic envelope membrane utilizing alternatives to traditional two-dimensional electrophoresis. J. Proteome Res. **2:** 413–425.

Garcia, O., Bouige, P., Forestier, C., and Dassa, E. (2004). Inventory and comparative analysis of rice and *Arabidopsis* ATP-binding cassette (ABC) systems. J. Mol. Biol. **343:** 249–265.

Gerdes, L., Bals, T., Klostermann, E., Karl, M., Philippar, K., Hunken, M., Soll, J., and Schunemann, D. (2006). A second thylakoid membrane-localized Alb3/OxaI/YidC homologue is involved in proper chloroplast biogenesis in *Arabidopsis thaliana*. J. Biol. Chem. **281:** 16632–16642.

Gietz, R.D., and Schiestl, R.H. (1991). Applications of high efficiency lithium acetate transformation of intact yeast cells using single-stranded nucleic acids as carrier. Yeast **7:** 253–263.

Hall, J.L., and Williams, L.E. (2003). Transition metal transporters in plants. J. Exp. Bot. **54:** 2601–2613.

Henriques, R., Jasik, J., Klein, M., Martinoia, E., Feller, U., Schell, J., Pais, M.S., and Koncz, C. (2002). Knock-out of *Arabidopsis* metal transporter gene IRT1 results in iron deficiency accompanied by cell differentiation defects. Plant Mol. Biol. **50:** 587–597.

Higgins, C.F. (2001). ABC transporters. Physiology, structure and mechanism—An overview. Res. Microbiol. **152:** 205–210.

Hirsch, J., Marin, E., Floriani, M., Chiarenza, S., Richaud, P., Nussaume, L., and Thibaud, M.C. (2006). Phosphate deficiency promotes modification of iron distribution in *Arabidopsis* plants. Biochimie **88:** 1767–1771.

Kaiser, B.N., Moreau, S., Castelli, J., Thomson, R., Lambert, A., Bogliolo, S., Puppo, A., and Day, D.A. (2003). The soybean NRAMP homologue, GmDMT1, is a symbiotic divalent metal transporter capable of ferrous iron transport. Plant J. **35:** 295–304.

Karimi, M., Inze, D., and Depicker, A. (2002). GATEWAY vectors for Agrobacterium-mediated plant transformation. Trends Plant Sci. **7:** 193–195.

Kliebenstein, D.J., Monde, R.A., and Last, R.L. (1998). Superoxide dismutase in Arabidopsis: An eclectic enzyme family with disparate regulation and protein localization. Plant Physiol. **118:** 637–650.

Korshunova, Y.O., Eide, D., Clark, W.G., Guerinot, M.L., and Pakrasi, H.B. (1999). The IRT1 protein from *Arabidopsis thaliana* is a metal transporter with a broad substrate range. Plant Mol. Biol. **40:** 37–44.

Lanquar, V., Lelievre, F., Bolte, S., Hames, C., Alcon, C., Neumann, D., Vansuyt, G., Curie, C., Schroder, A., Kramer, U., Barbier-Brygoo, H., and Thomine, S. (2005). Mobilization of vacuolar iron by AtNRAMP3 and AtNRAMP4 is essential for seed germination on low iron. EMBO J. **24:** 4041–4051.

Lee, Y.J., Kim, D.H., Kim, Y.W., and Hwang, I. (2001). Identification of a signal that distinguishes between the chloroplast outer envelope membrane and the endomembrane system in vivo. Plant Cell **13:** 2175–2190.

Le Jean, M., Schikora, A., Mari, S., Briat, J.F., and Curie, C. (2005). A loss-of-function mutation in AtYSL1 reveals its role in iron and nicotianamine seed loading. Plant J. **44:** 769–782.

Matsuzaki, M., et al. (2004). Genome sequence of the ultrasmall unicellular red alga *Cyanidioschyzon merolae* 10D. Nature **428:** 653–657.

Möller, S.G., ed (2005). Plastids. (Oxford, UK: Blackwell Publishing).

Murcha, M.W., Elhafez, D., Lister, R., Tonti-Filippini, J., Baumgartner, M., Philippar, K., Carrie, C., Mokranjac, D., Soll, J., and Whelan, J. (2007). Characterisation of the preprotein and amino acid transporter gene family in Arabidopsis. Plant Physiol. **143:** 199–212.

Nada, A., and Soll, J. (2004). Inner envelope protein 32 is imported into chloroplasts by a novel pathway. J. Cell Sci. **117:** 3975–3982.

Nakamura, Y., et al. (2003). Complete genome structure of *Gloeobacter violaceus* PCC 7421, a cyanobacterium that lacks thylakoids. DNA Res. **10:** 137–145.

Nishiyama, T., et al. (2003). Comparative genomics of *Physcomitrella patens* gametophytic transcriptome and *Arabidopsis thaliana*: Implication for land plant evolution. Proc. Natl. Acad. Sci. USA **100:** 8007–8012.

Philippar, K., Ivashikina, N., Ache, P., Christian, M., Luthen, H., Palme, K., and Hedrich, R. (2004). Auxin activates KAT1 and KAT2, two K+-channel genes expressed in seedlings of *Arabidopsis thaliana*. Plant J. **37:** 815–827.

Raux-Deery, E., Leech, H.K., Nakrieko, K.A., McLean, K.J., Munro, A.W., Heathcote, P., Rigby, S.E.J., Smith, A.G., and Warren, M.J.

(2005). Identification and characterization of the terminal enzyme of siroheme biosynthesis from *Arabidopsis thaliana*. J. Biol. Chem. **280:** 4713–4721.

Raven, J.A., Evans, M.C.E., and Korb, R.E. (1999). The role of trace metals in photosynthetic electron transport in O_2-evolving organisms. Photosynth. Res. **60:** 111–149.

Reese, M.G. (2001). Application of a time-delay neural network to promoter annotation in the *Drosophila melanogaster* genome. Comput. Chem. **26:** 51–56.

Robinson, N.J., Procter, C.M., Connolly, E.L., and Guerinot, M.L. (1999). A ferric-chelate reductase for iron uptake from soils. Nature **397:** 694–697.

Rolland, N., Ferro, M., Seigneurin-Berny, D., Garin, J., Douce, R., and Joyard, J. (2003). Proteomics of chloroplast envelope membranes. Photosynth. Res. **78:** 205–230.

Rosso, M.G., Li, Y., Strizhov, N., Reiss, B., Dekker, K., and Weisshaar, B. (2003). An *Arabidopsis thaliana* T-DNA mutagenized population (GABI-Kat) for flanking sequence tag-based reverse genetics. Plant Mol. Biol. **53:** 247–259.

Schmid, M., Davison, T.S., Henz, S.R., Pape, U.J., Demar, M., Vingron, M., Scholkopf, B., Weigel, D., and Lohmann, J.U. (2005). A gene expression map of *Arabidopsis thaliana* development. Nat. Genet. **37:** 501–506.

Schwacke, R., Schneider, A., van der Graaff, E., Fischer, K., Catoni, E., Desimone, M., Frommer, W.B., Flugge, U.I., and Kunze, R. (2003). ARAMEMNON, a novel database for Arabidopsis integral membrane proteins. Plant Physiol. **131:** 16–26.

Seigneurin-Berny, D., et al. (2006). HMA1, a new Cu-ATPase of the chloroplast envelope, is essential for growth under adverse light conditions. J. Biol. Chem. **182:** 2882–2892.

Shikanai, T., Muller-Moule, P., Munekage, Y., Niyogi, K.K., and Pilon, M. (2003). PAA1, a P-type ATPase of *Arabidopsis*, functions in copper transport in chloroplasts. Plant Cell **15:** 1333–1346.

Shingles, R., North, M., and McCarty, R.E. (2001). Direct measurement of ferrous ion transport across membranes using a sensitive fluorometric assay. Anal. Biochem. **296:** 106–113.

Shingles, R., North, M., and McCarty, R.E. (2002). Ferrous ion transport across chloroplast inner envelope membranes. Plant Physiol. **128:** 1022–1030.

Spurr, A.R. (1969). A low-viscosity epoxy resin embedding medium for electron microscopy. J. Ultrastruct. Res. **26:** 31–43.

Swofford, D.L. (2002). PAUP*. Phylogenetic Analysis Using Parsimony *and Other Methods, Version 4. (Sunderland, MA: Sinauer Associates).

Talke, I.N., Hanikenne, M., and Krämer, U. (2006). Zinc-dependent global transcriptional control, transcriptional deregulation, and higher gene copy number for genes in metal homeostasis of the hyperaccumulator *Arabidopsis halleri*. Plant Physiol. **142:** 148–167.

Tatusov, R., et al. (2003). The COG database: An updated version includes eukaryotes. BMC Bioinformatics **4:** 41.

Teng, Y.S., Su, Y.S., Chen, L.J., Lee, Y.J., Hwang, I., and Li, H.M. (2006). Tic21 is an essential translocon component for protein translocation across the chloroplast inner envelope membrane. Plant Cell **18:** 2247–2257.

Thomine, S., Lelievre, F., Debarbieux, E., Schroeder, J.I., and Barbier-Brygoo, H. (2003). AtNRAMP3, a multispecific vacuolar metal transporter involved in plant responses to iron deficiency. Plant J. **34:** 685–695.

Thomine, S., Wang, R., Ward, J.M., Crawford, N.M., and Schroeder, J.I. (2000). Cadmium and iron transport by members of a plant metal transporter family in *Arabidopsis* with homology to *Nramp* genes. Proc. Natl. Acad. Sci. USA **97:** 4991–4996.

Thompson, J.D., Gibson, T.J., Plewniak, F., Jeanmougin, F., and Higgins, D.G. (1997). The CLUSTAL_X windows interface: Flexible strategies for multiple sequence alignment aided by quality analysis tools. Nucleic Acids Res. **25:** 4876–4882.

Tusher, V.G., Tibshirani, R., and Chu, G. (2001). Significance analysis of microarrays applied to the ionizing radiation response. Proc. Natl. Acad. Sci. USA **98:** 5116–5121.

Van Wuytswinkel, O., Vansuyt, G., Grignon, N., Fourcroy, P., and Briat, J.F. (1998). Iron homeostasis alteration in transgenic tobacco overexpressing ferritin. Plant J. **17:** 93–97.

Varotto, C., Maiwald, D., Pesaresi, P., Jahns, P., Salamini, F., and Leister, D. (2002). The metal ion transporter IRT1 is necessary for iron homeostasis and efficient photosynthesis in *Arabidopsis thaliana*. Plant J. **31:** 589–599.

Vert, G., Grotz, N., Dedaldechamp, F., Gaymard, F., Guerinot, M.L., Briat, J.F., and Curie, C. (2002). IRT1, an *Arabidopsis* transporter essential for iron uptake from the soil and for plant growth. Plant Cell **14:** 1223–1233.

Vert, G.A., Briat, J.F., and Curie, C. (2003). Dual regulation of the Arabidopsis high-affinity root iron uptake system by local and long-distance signals. Plant Physiol. **132:** 796–804.

Vothknecht, U.C., and Soll, J. (2005). Chloroplast membrane transport: Interplay of prokaryotic and eukaryotic traits. Gene **354:** 99–109.

Waters, B.M., Chu, H.H., DiDonato, R.J., Roberts, L.A., Eisley, R.B., Lahner, B., Salt, D.E., and Walker, E.L. (2006). Mutations in Arabidopsis Yellow Stripe-Like1 and Yellow Stripe-Like3 reveal their roles in metal ion homeostasis and loading of metal ions in seeds. Plant Physiol. **141:** 1446–1458.

Wintz, H., Fox, T., Wu, Y.Y., Feng, V., Chen, W., Chang, H.S., Zhu, T., and Vulpe, C. (2003). Expression profiles of *Arabidopsis thaliana* in mineral deficiencies reveal novel transporters involved in metal homeostasis. J. Biol. Chem. **278:** 47644–47653.

Yamada, K., et al. (2003). Empirical analysis of transcriptional activity in the *Arabidopsis* genome. Science **302:** 842–846.

Ye, H., Pilon, M., and Pilon-Smits, E.A.H. (2006). CpNifS-dependent iron-sulfur cluster biogenesis in chloroplasts. New Phytol. **171:** 285–292.